

Review

A Comprehensive Review on Hydrogen Absorption Behaviour of Metal Alloys Prepared through Mechanical Alloying

Thabang Ronny Somo ^{1,2}, Thabiso Carol Maponya ¹, Moegamat Wafeeq Davids ², Mpitloane Joseph Hato ^{1,*}, Mykhaylo Volodymyrovich Lototskyy ² and Kwena Desmond Modibane ^{1,*} 

¹ Nanotechnology Research Lab, Department of Chemistry, School of Physical and Mineral Sciences, University of Limpopo (Turfloop), Polokwane 0727, South Africa; somoronny@gmail.com (T.R.S.); thabiso.maponya@ul.ac.za (T.C.M.)

² Hydrogen South Africa (HySA), South African Institute of Advanced Chemistry, University of the Western Cape, Cape Town 7535, South Africa; 2235735@myuwc.ac.za (M.W.D.); mlototskyy@uwc.ac.za (M.V.L.)

* Correspondence: mpitloane.hato@ul.ac.za (M.J.H.); kwena.modibane@ul.ac.za (K.D.M.); Tel.: +27-(0)15-268-4116 (M.J.H.); +27-(0)15-268-3783 (K.D.M.)

Received: 21 March 2020; Accepted: 18 April 2020; Published: 26 April 2020



Abstract: Hydride-forming alloys are currently considered reliable and suitable hydrogen storage materials because of their relatively high volumetric densities, and reversible H₂ absorption/desorption kinetics, with high storage capacity. Nonetheless, their practical use is obstructed by several factors, including deterioration and slow hydrogen absorption/desorption kinetics resulting from the surface chemical action of gas impurities. Lately, common strategies, such as spark plasma sintering, mechanical alloying, melt spinning, surface modification and alloying with other elements have been exploited, in order to overcome kinetic barriers. Through these techniques, improvements in hydriding kinetics has been achieved, however, it is still far from that required in practical application. In this review, we provide a critical overview on the effect of mechanical alloying of various metal hydrides (MHs), ranging from binary hydrides (CaH₂, MgH₂, etc) to ternary hydrides (examples being Ti-Mn-N and Ca-La-Mg-based systems), that are used in solid-state hydrogen storage, while we also deliver comparative study on how the aforementioned alloy preparation techniques affect H₂ absorption/desorption kinetics of different MHs. Comparisons have been made on the resultant material phases attained by mechanical alloying with those of melt spinning and spark plasma sintering techniques. The reaction mechanism, surface modification techniques and hydrogen storage properties of these various MHs were discussed in detail. We also discussed the remaining challenges and proposed some suggestions to the emerging research of MHs. Based on the findings obtained in this review, the combination of two or more compatible techniques, e.g., synthesis of metal alloy materials through mechanical alloying followed by surface modification (metal deposition, metal-metal co-deposition or fluorination), may provide better hydriding kinetics.

Keywords: metal hydrides; hydrogen storage; hydriding kinetics; surface modification; mechanical alloying

1. Introduction

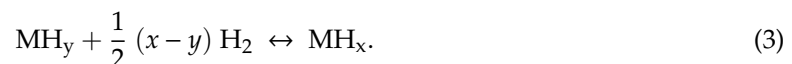
The physical storage of hydrogen through compressed H₂ tanks, liquid H₂ tanks and cryo-compressed tanks has been condemned, due to several limitations, including the high pressure required for compression of the hydrogen gas and a large amount of energy for liquefaction of hydrogen [1]. A convenient way to store hydrogen is through the absorption of hydrogen onto solid

nanostructured materials such as metal alloys, chemical sorbents (metal organic frameworks (MOFs) and carbon-based materials) or chemical hydrides [2]. Out of the above-mentioned chemical storage materials, metal hydrides offer a safe, volume-efficient technology aimed at hydrogen storage for reversible on-board applications due to their large hydrogen uptake capacity (7.6 wt. % by Mg-type alloys) [3,4]. There are excellent reviews, regarding MHs, prepared by equilibrium procedure for hydrogen storage application that have been published [4–6]. However, there are not a lot of reviews on the MHs prepared by non-equilibrium procedure.

It is well-documented that metallic hydrides are chemically formed from the reaction of hydrogen gas with metal or alloy according to Equation (1) [1]:



The formation of metal hydride undergoes six distinct states of hydrogen absorption in metals: Hydrogen to metal; physisorption, which involves physical attachment of hydrogen to a metal through van der Waals interaction; chemisorption, the chemical attachment of hydrogen to metal by forming a chemical bond; subsurface hydrogen; solid solution (α -phase) and hydride (β -phase) [7]. The formation of α - and β -phases may be described by Equations (2) and (3), respectively [8]. An α -phase is formed when small amount of hydrogen occupies the interstitial sites of the host metal M, producing an H-poor solid solution, while β -phase involves saturation of the solid solution to generate a second phase:



Where M represents metal and H represents hydrogen atoms. During the formation of β -phase, the equilibrium pressure is fixed at any given temperature. According to Gibbs' phase rule ($F = C - P + 2$, in which F is degrees of freedom, C represent the components of a reaction and P is the number of phases), the number of degrees of freedom, F , is one during the interaction of metal (M) and hydrogen (H) atoms since three phases P (two solid and one gaseous) and two components C (H and M) are available [8]. The constant pressure level is referred to as the plateau pressure. During the formation, the metal atoms stretch apart to accommodate the hydrogen atoms and the physical structure of the metal atoms may also change to form a metal hydride. For example, Table 1 shows different types of metal alloys ranging from AB to AB₅, demonstrating that hydrogenation of metal is accompanied by increase in lattice parameters of the parent alloy [9–13]. The A₂B alloys were reported to possess higher hydrogen storage capacity of 3.75 and 3.04 wt. % for P6222, and Fddd phase, respectively [11]. On the other hand, AB₅ showed to have low absorption capacity of 1.43 wt. % [10]. Moreover, peaks from X-ray diffractogram may broaden and shift towards smaller 2θ values as a result of larger lattice parameters [9].

Conversely, metal hydrides release H₂ gas when heat is applied on the hydride. This process is called desorption. Hydrogen atoms (H) move from the metal to the surface of the material, combine into hydrogen molecules (H₂) and flow away as hydrogen gas. The metal atoms contract to form its original metal crystal structure [14]. The metal alloys in Table 1 can easily be synthesized by a well-known equilibrium procedure called arc or induction melting [15,16]. However, alloys prepared through this method suffer from poor hydrogenation performances and poisoning intolerance [17]. Recent findings reported that a convenient way to overcome some of these challenges is to prepare metal alloys using mechanical alloying (MA) through high-energy ball milling technique [15,18]. In this review, we provide the recent developments on hydrogenation performances of metal alloys prepared by mechanical alloying technique, comparison of MA with other non-equilibrium techniques. Moreover, we also consider the effect of combining MA with some surface modification technologies.

We anticipate that this work can provide an inspiring perspective for further research on MHs with good hydrogen storage properties.

Table 1. Lattice parameter, a , of different types of alloys before and after hydrogenation and their hydrogen storage capacities.

Type of Alloy	Structure	Alloy Lattice Parameter, a , Å	Hydride Lattice Parameter, a , Å	Storage Capacity, wt. %	References
AB	BCC	2.976	7.029	1.75	[12]
AB ₂	C14	4.866	4.902	1.70	[13]
	C15	6.939	7.158	2.01	[11]
AB ₅	CaCu ₅	5.003	5.395	1.43	[10]
A ₂ B	(P6222)	5.205	5.463	3.75	[11]
	(Fddd)	5.284	5.411	3.04	[11]

2. Non-Equilibrium Preparation Techniques

Mechanical, kinetic and thermodynamic performances related to the formation of metal hydride are affected by structure and phases of metal or metal alloy of interest. It is currently well-known that the structure and phase of alloy materials can be controlled by synthesizing them under non-equilibrium conditions [19]. There are several processes/techniques, which are in commercial use for the synthesis of alloy materials under such conditions. Amongst such techniques, much attention has been given to mechanical alloying, melt spinning and spark plasma sintering techniques [20]. According to Scudino et al. [21], the general underlying idea in all these techniques is to synthesize alloy materials in a non-equilibrium state by “energizing and quenching”. The energizing process involves the use of external dynamical force, such as melting; evaporation; irradiation; application of pressure; or storing of mechanical energy by plastic deformation on solid-state materials to put them onto a non-equilibrium state [22]. During this process, the solid-state materials change in phase to gas or liquid. In “quenching”, a subsequent step after “energization”, the material of interest is extinguished into a frozen state, and it is at this point where the desired structure or phase can be easily controlled [23,24]. The alloys synthesized in this sequence possess particular structural characteristics that are difficult or rare to attain by equilibrium preparation methods: Nano-crystalline grain size with a high density of grain boundaries and even lacking of long-range order (amorphous state). These structures alloy quick hydrogen uptake and excellent cycle-life behaviour [25]. Among all preparation methods that follow “energizing and quenching” mechanism, MA has been given much attention due to its user-friendly, comparatively less costly machinery and applicability to various metal alloys [19]. In this regard, mechanical alloying experimental technique is discussed with the point of interest being its effect on hydrogenation performances of metal alloy materials.

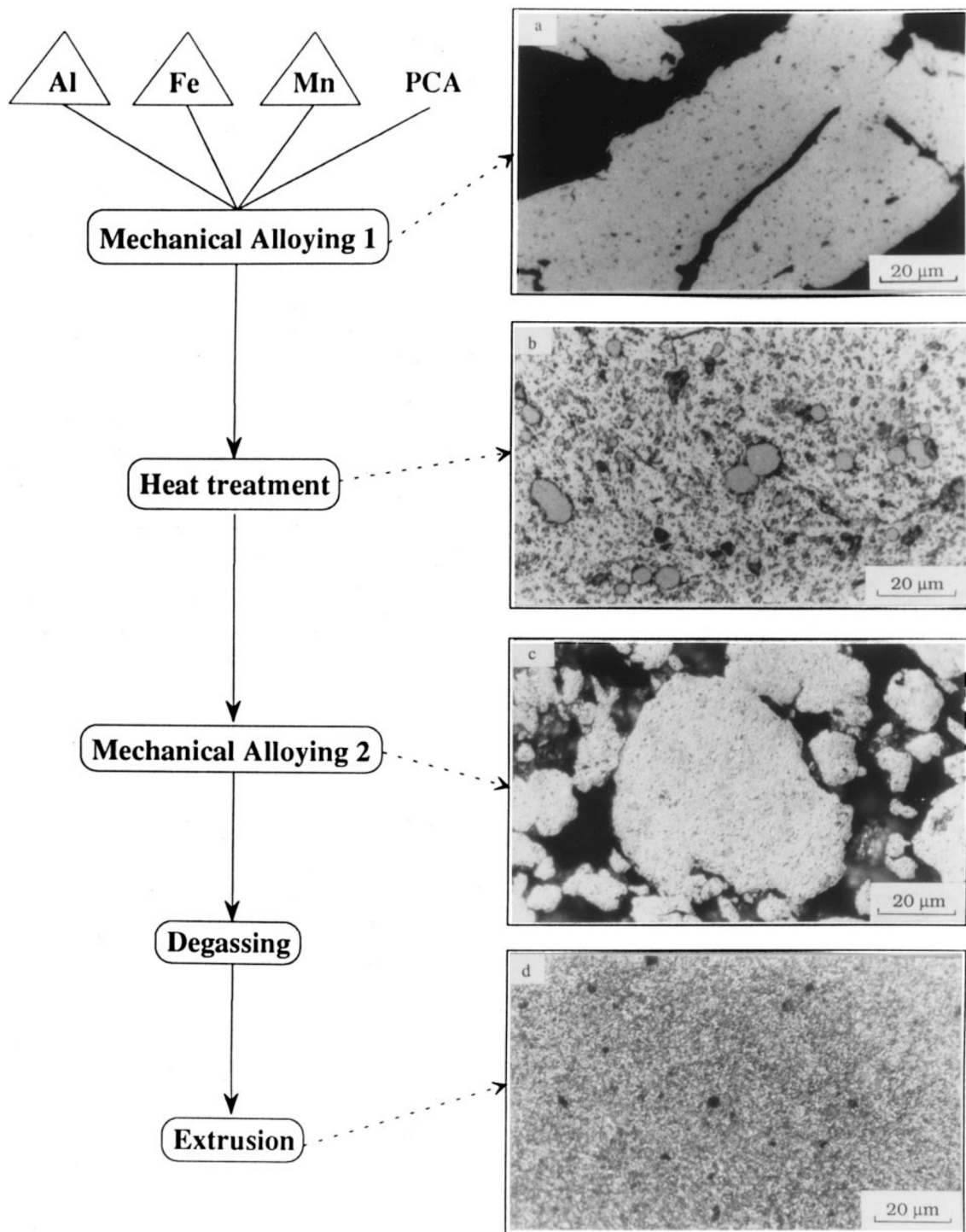


Figure 1. Process flowsheet and the microstructures developed during double mechanical alloying of an Al-5wt.%Fe-4wt.%Mn powder mixture, reproduced from [19], with permission from Elsevier, 2001.

3. Mechanical Alloying

3.1. Background

Mechanical alloying, also known as ball milling, is a solid-state powder processing technique involving repeated welding, fracturing, and rewelding of powder particles in a high-energy ball mill [19]. Repetitions of welding, as well as fracturing of particles, generate a lamellar structure

within the powders. MA method is usually applied when synthesizing highly immiscible phases in a non-equilibrium state [26]. The immiscible phases that are prepared, include super-saturated solid solutions, non-equilibrium alloys that are usually amorphous in nature, metastable crystalline and quasicrystalline phases. The procedure of MA begins with blending of the powders in the correct extent and stacking the powder blend into the mill along with the grinding medium. This blend is then milled for the ideal time allotment until a consistent state is achieved when the arrangement of each powder particle is equivalent to the extent of the elements in the initial powder blend. The milled powder is then united into a mass shape and exposed to heat, in order to get the ideal phase and structure. Thus, the vital components of MA procedure are the raw materials, mill and procedure parameters. This procedure was described by Shang et al. [27]. Ares et al. [25] observed that diffraction peaks from the X-ray diffractogram (XRD) of $Mm(Ni, Mn, Al, Co)_{5.2}$ became broader with milling time. An example of MA process is depicted in Figure 1 (synthesis of Al–5wt. %Fe–4wt. %Mn blend), with scanning electron microscopic (SEM) images provided for all the steps. The double mechanical milling, as observed in the figure is necessary to refine the intermetallics and decrease the particle size of the blend [19]. MA has also been utilized to synthesize AB (FeTi), A_2B (Mg_2Ni) and AB_5 (binary $LaNi_5$) alloys [28]. In most cases, the rate of hydrogenation has been greatly enhanced when compared with that of materials prepared through conventional equilibrium methods, but due to the amorphous nature of milled alloys, a loss of hydrogen content was observed [25]. MA provides various advantages, including smaller restrictions with respect to composition and works much better when applied to A_2B alloys [29]. Moreover, through the use of MA method, nano-crystalline alloys are obtained, starting either with a pre-prepared alloy or with a mixture of pure elemental metals [28]. Nano-crystalline alloys that are prepared through MA technique possess better activation compared to their polycrystalline counterparts [28]. For example, Polycrystalline FeTi is activated by heating up to temperatures above 673 K for one to two hours followed by annealing at 7 bar pressure and its hydrogenation requires a high pressure of 40–70 bar [30]. However, with a mechanically-alloyed nano-crystalline FeTi alloy, a single vacuum heating at 673 K for 30 min is sufficient to obtain full hydrogen absorption cycles [30].

3.2. Mg-Based Alloys

3.2.1. Structural Characteristics of Mechanically Milled Mg-Based Alloys

The crystal structure of a metallic Mg is hexagonal with lattice parameters $a = 3.2094 \text{ \AA}$ and $c = 5.2108 \text{ \AA}$ and a space group of P63/mmc [31]. Formation of MgH_2 hydride consists of two steps, i.e., preparation of Mg nanoparticles, followed by hydrogen absorption to form the metal hydride. A traditional method for preparing Mg nanoparticles is gas-phase condensation method, which is much better discussed in [32]. As depicted by Figure 2a, hydrogenation of Mg nanoparticles tempers with XRD diffraction pattern of the parent nanoparticles [33]. Diffraction peaks at $2\theta \approx 48^\circ$, 34° and 32° disappear, while several new peaks develop, forming tetragonal magnesium hydride (β - MgH_2) phase [33]. To illustrate the difference between traditionally synthesized MgH_2 hydride and those synthesized through mechanical/ball milling, XRD diffraction patterns of MgH_2 and as-milled hydrided Mg-Al alloy are compared in Figure 2a,b, respectively. For as-milled Mg-Al alloy, Li et al. [31] reported four stable phases: the fcc solid solution of magnesium in aluminum, the hcp solid solution of aluminum in magnesium, the β -phase (Mg_2Al_3) and the γ -phase ($Mg_{17}Al_{12}$). Such rewarding characteristic gives rise to excellent hydriding behavior of as-milled Mg-based alloys.

In general, the morphology and particle size distribution are also important structural parameters, carrying a huge responsibility for surface physisorption of molecular hydrogen (H_2), surface dissociative chemisorption, surface absorption, hydrogen diffusion and phase transformation [34]. These two parameters are well-interpreted using scanning electron microscopic (SEM) images. For Mg-based alloys, mechanically milled alloys show faster hydrogen absorption kinetics and larger uptake capacity, compared to their unmilled counterparts and one of the effective factors contributing to this, is the

reduction of particle sizes of the parent materials during mechanical alloying [35]. According to the literature, small particle sizes allow easy mobility of molecular hydrogen and quick dissociation into atomic hydrogen on the surface of a material [33]. As shown in Figure 3, all the five SEM images of milled Mg-based alloys constitute of smaller particles than that of traditionally synthesized MgH_2 , [33]. Therefore, their hydrogen uptake performance is expected to be superior to that of MgH_2 . This is further discussed in the next section.

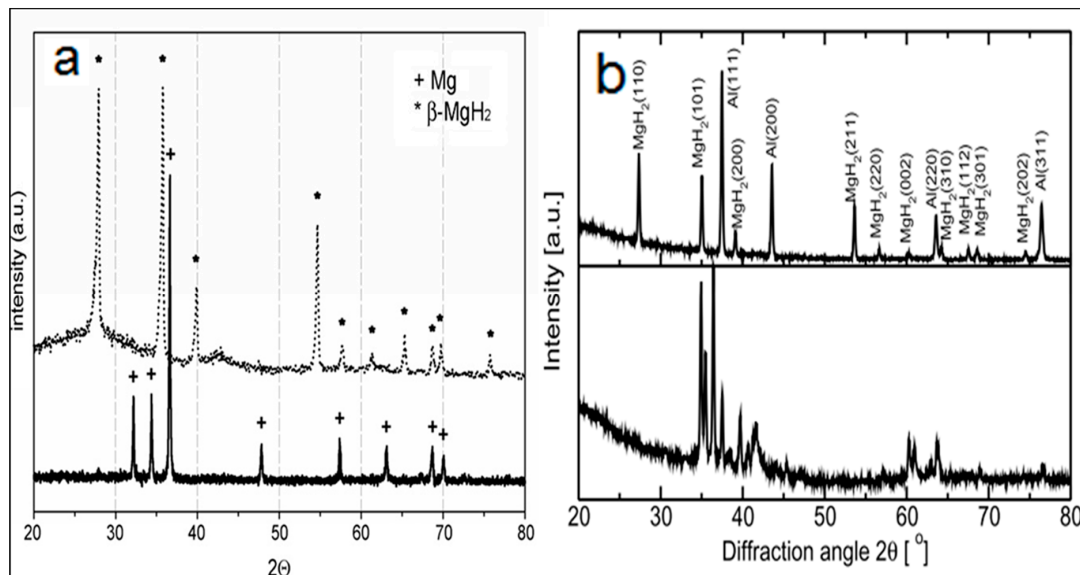


Figure 2. XRD diffraction patterns of (a) nanocrystalline Mg and MgH_2 , and (b) Mg-Al alloy in the hydrogenated state (top) and dehydrogenated state (bottom). Figures reproduced from [33], and [31], respectively, [31] with permission from Elsevier, 2008; [33] with permission from Elsevier, 2007.

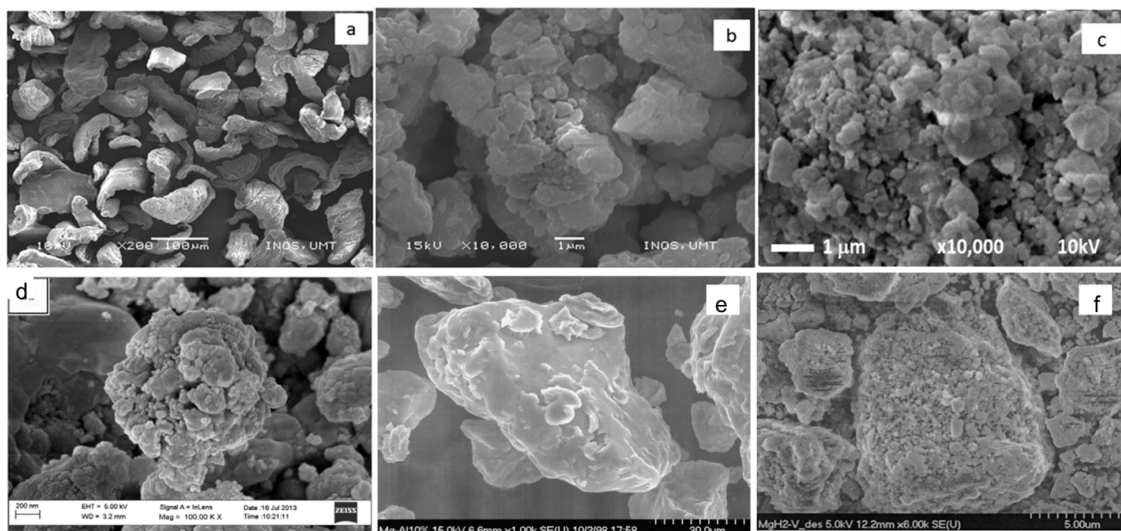


Figure 3. The SEM images of the (a) MgH_2 , (b) as-milled MgH_2 , (c) as-milled MgH_2 + 10wt. % $CeCl_3$, (d) as-milled Mg-10 $FeTiO_3$, (e) as-milled Mg:Al (90:10) and (f) as-milled MgH-5 at. % V. Figures (a–c) were reprinted with permission from [36], with permission from Elsevier, 2016 (d) reproduced from [37], with permission from Elsevier, 2015; (e) reproduced from [38], with permission from Elsevier, 2000 and (f) reproduced from [39], with permission from Elsevier, 1999.

3.2.2. Hydrogen Absorption Behaviour of Mechanically Alloyed Mg-Based Alloys

Mg-based alloys are reported to possess energy density of 9 MJ/kg and the highest maximum hydrogen storage capacity (7.6 and 3.6 wt. % for MgH₂, and Mg₂NiH₄, respectively) compared to all hydride-forming materials [40,41]. The hydride stability of this alloy is very high, and therefore, a high dissociation temperature of around 561 K is required to transform MgH₂ hydride into Mg and H₂ gas [42]. Furthermore, the hydriding kinetics of MgH₂ hydride is relatively slow because the dissociation of molecular hydrogen into hydrogen atoms is difficult on the surface of Mg metal [43]. Several reports are found in the literature concerning synthesis and hydrogen properties of Mg-based alloys synthesized by mechanical alloying [3,44–46]. Another interesting study is Andreassen [31]. The authors' work was based on the comparison of hydrogen kinetics, presented in Figure 4a, of un-milled Mg and those of ball milled Mg-Al compounds with varying Al content [31]. The kinetics increased gradually with an increase in Al content due to easy dissociation of hydrogen molecules on the surface of Al, as a result of negligible activation barrier for hydrogen dissociation for this metal. It is, therefore, understood that hydrogen molecules split into atomic hydrogen on the surface of Al before diffusing and attaching on the active sites of Mg, which has higher hydrogen sticking ability compared to Al [31]. Lototskyy et al. [37] reported the effect of synthesizing different Mg-based composites varying the amounts of multi-walled carbon nanotubes, activated carbon, FeTiO₃ and graphite using mechanical alloying at a rotation speed of 500 rpm for a period of 120 min on hydrogenation behaviour of Mg, Figure 4b. The authors discovered that hydrogenation behaviour (both the uptake capacity and kinetics) of Mg mechanically alloyed with carbon-based materials are exceptional. Ref. [46] reveals that the better hydrogenation behaviour possessed by milled alloys can be attributed to their combination of tetragonal (a = 4.52 Å, c = 3.02 Å) and orthorhombic (a = 4.48 Å, b = 5.40 Å, c = 4.90 Å) phases as major phases, since these two phases are associated with small particle size and a presence of strain in the particles. Similar trends of hydrogen capacity and kinetics were observed by Lototskyy et al. [47] and Williams et al. [48] when they assessed Mg-10(FeV)-5MWCNT and Mg-5Pd composites through mechanical alloying, respectively. Tables 2 and 3 represent a compiled data of literature based on hydrogenation behaviour of Mg-based alloy materials synthesized through ball milling and mechanical alloying.

Table 2. Thermodynamic and kinetic properties of ball-milled MgH₂ doped with catalytic additives.

Catalyst Family	Catalyst Additive	ΔH_{des} , kJ/mol H ₂	Hydriding Kinetics, min ⁻¹	Hydrogen Capacity, wt. %	References
No catalyst	Undoped MgH ₂	76	1.4×10^{-3}	7.66	[52,57]
Metal	MgH ₂ +10 wt. % Ni	75	–	6.89	[49]
	MgH ₂ +10 wt. % Co	71	–	5.62	[49]
Metal halides	MgH ₂ +10 wt. % CeCl ₃	75.7	0.05	6.32	[36]
	MgH ₂ +NbF ₅	79.7	3.42	6.40	[53]
	MgH ₂ +ZrF ₄	76.4	3.2	6.44	[53]
Hydrides	MgH ₂ +NaAlH ₄	–	0.28	3.10	[49]
Metal oxide	MgH ₂ +SrTiO ₃	–	0.02	6.63	[50]
	MgH ₂ +1 mol. % Nb ₂ O ₅	74	0.22	5.45	[51]
Nano-sized alloys	MgH ₂ +10 wt. % Zr ₂ Ni	–	0.52	5.12	[55]
	MgH ₂ +FeNb	–	0.35	5.55	[56]
Carbon materials	MgH ₂ +5 wt. %SWNT	–	1.34	6.72	[54]

ΔH_{des} = Enthalpy of desorption*SWNT = Single-walled carbon nanotube.

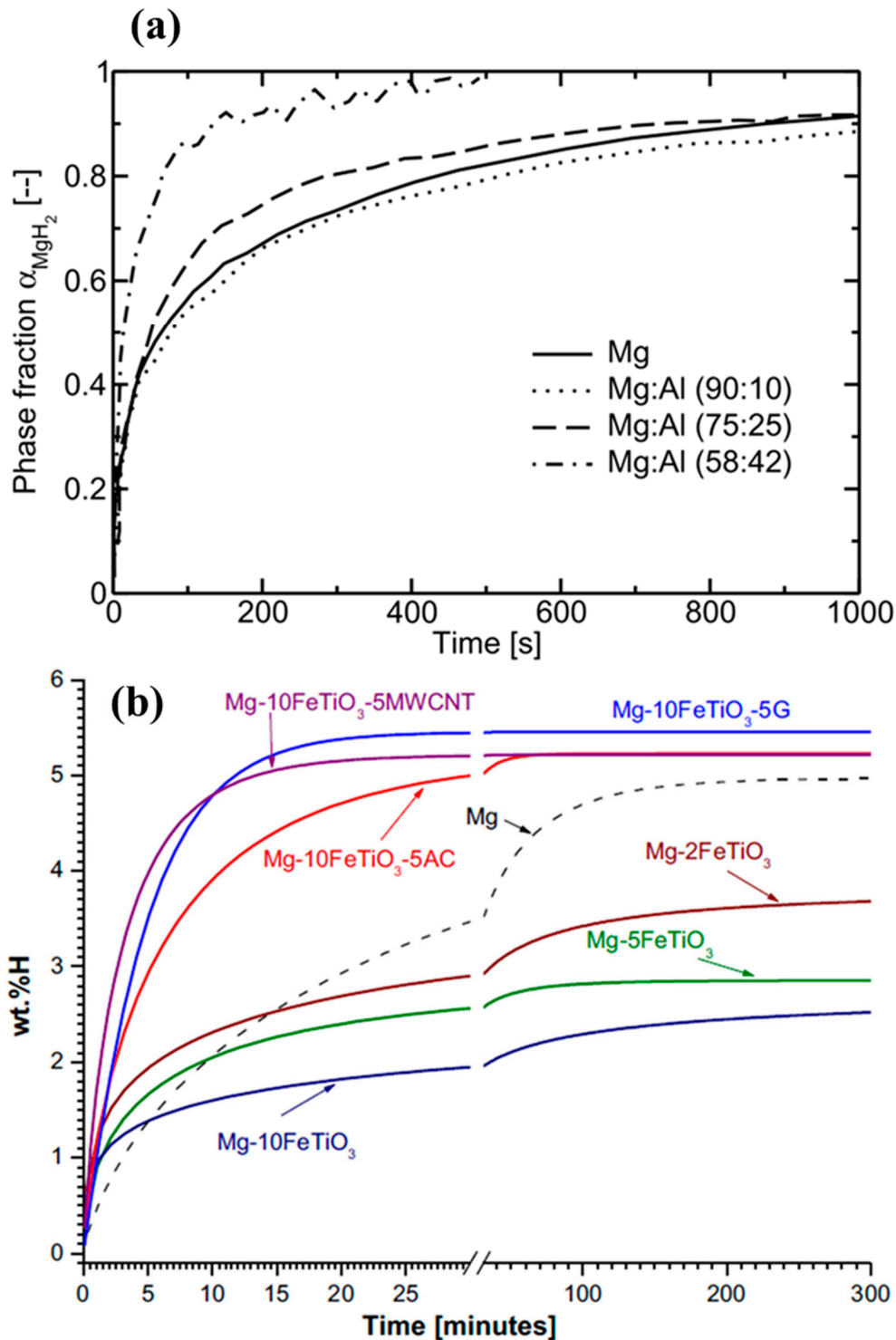


Figure 4. (a) Hydrogenation kinetics of pure un-milled Mg compared with Mg-Al compounds with varying Al content ball milled for 20 h. Hydrogenation performed at $T = 400\text{ }^\circ\text{C}$ and a hydrogen pressure of 38 bar. Data extracted from ref. [31], with permission from Elsevier, 2008. (b) Hydrogenation kinetics of Mg and its carbon-based composites (15 bar and $\text{H}_2/250\text{ }^\circ\text{C}$), reproduced from [37], with permission from Elsevier, 2015.

3.2.3. Ball-Milled MgH_2 Doped with Catalytic Additives

In the previous section, much attention is given to mechanically milled Mg-based alloys where a pure milled/un-milled Mg metal is admixed with other several materials, such as FeTiO_3 before

their interaction with hydrogen is subsequently explored. Here, we discuss the influence of catalytic effect of doping ball milled MgH_2 with different catalytic additives. Previous experiments indicate clearly that admixing, deposition or doping of catalysts and additives could greatly enhance thermodynamic property and de/rehydrogenation kinetic parameters of MgH_2 . In these studies, metal [49], metal oxide [50–52], metal halides [36,53], metal hydride [49], carbon materials [54] and nanosized alloys [55,56] were used as the catalysts and additives. Table 2 summarizes thermodynamic and kinetic effects of these catalysts. The materials in the table were prepared through ball milling technique.

We can conclude from the table that doped MgH_2 materials, prepared through mechanical milling, enjoy superior hydrogenation kinetics, compared to undoped materials. However, this particular excellent improvement significantly reduces the maximum absorption capacity of the system. For metal halide family, particularly $\text{MgH}_2+10\text{wt. \%CeCl}_3$, the loss of capacity can be related to in situ formation of CeMg alloy and MgCl_2 , which seem to be good catalysts for faster absorption but poor gas absorbers [53]. On the other hand, drastic decrease of absorption capacity revealed by MgH_2+SWNT composite is suggested to come from structure destruction of the SWNT during milling [54]. Table 2 also shows that composites which resulted in major decrease in hydrogen capacity are those with a dopant of 10 wt. % or more. We therefore suggest preparation of MgH_2 composites with dopants that are less than a concentration of 10 wt. %. Moreover, milling period should also be taken into consideration when these materials are formed, more especially when carbon materials are in abundance as they seem to be sensitive to milling conditions. The difference between enthalpy of desorption (ΔH_{des}) of the materials is negligible and as thus thermodynamic property of MgH_2 remain unchanged upon doping.

3.3. AB_5 -Type Alloys

3.3.1. Structural Characteristics of Mechanically Milled AB_5 -Type Alloys

Another interesting class of metal alloys is AB_5 . The A site in AB_5 represents one or more strongly hydride-forming elements while B site represents one or more weakly hydride-forming elements, and usually helps to dissociate the H_2 molecules on the surface of alloy material [58]. The A site is usually occupied by La, Ca or rare earth element while Ni, Cu, Co, Pt or Fe fill the B site [59]. AB_5 alloys are known to have a CuCa_5 -type hexagonal crystal structure which normally belongs to space group $P6/mmm$ (#191) [60,61]. Singh et al. [62] evaluated the effect of milling $\text{MmNi}_{4.6}\text{Fe}_{0.4}$ alloy, where Mm refers to mischmetal, varying the milling period from 10, 20 and 30 min, at a milling speed of 200 rpm. As shown by Figure 5, mechanical milling of this alloy results in slight shift of diffraction peaks towards lower 2θ values, reflecting increase in lattice parameters, and peak width broadening. Peak width broadening is a reflection of decrease in particle size. In general, the lattice structure of MmNi_5 -type alloy consists of two stacked planes at $z = 0$ and $z = \frac{1}{2}$, and the first plane contains 1a and 2c, while the latter plane contains 3g crystallographic sites. Both Mm and Ni atoms occupy the 1a and 2c sites, while the 3g sites are occupied by Ni atoms only. Therefore in the presence of Fe to form $\text{MmNi}_{4.6}\text{Fe}_{0.4}$ alloy, Fe atoms replace Ni on the 3g sites [63]. Electronic configuration of Fe and that of Ni are very close ($3d^64s^2$ for Fe and $3d^84s^2$ for Ni) and as a result covalent character, which is stronger than ionic character, is expected in the Ni/Fe-bearing planes. Thus, during mechanical milling of an alloy material with such character, strained platelet shaped particles are expected to form [64]. Such particles allow smooth movement of hydrogen during sorption better than fine powdered particles. This statement is supported by Table 3 as it is observed from the table that materials that were milled for longer period of time are associated with lower hydrogen uptake capacity compared to their counterparts that were milled for shorter period. This is due to the mechanical energy that is being pumped into the alloy matrix during milling, which breaks the particles, while forming strain in the matrix, and thus, for longer milling periods fractured and much finer powders, which are not recommended may result [63,64].

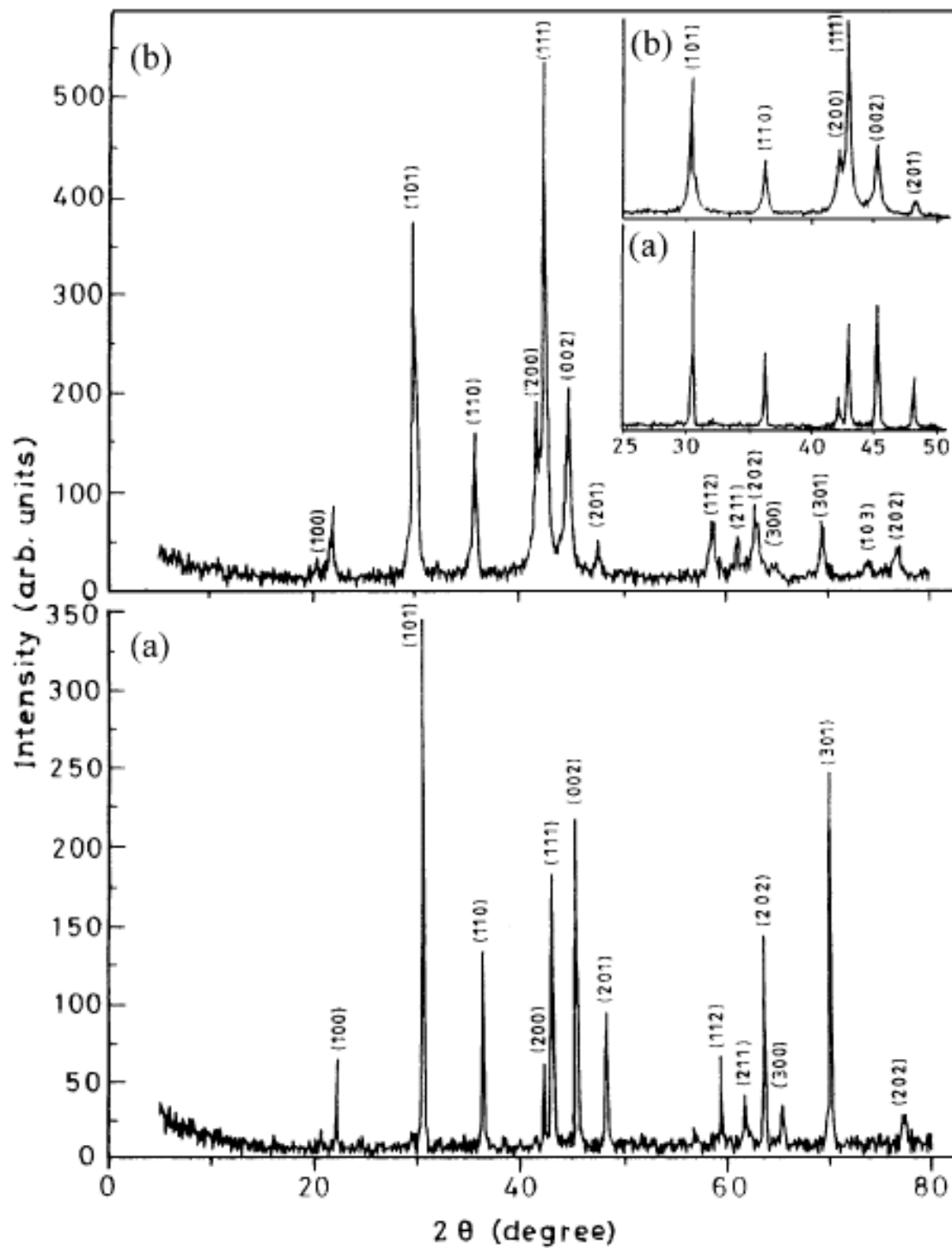


Figure 5. X-ray diffractograms of the unmillied; (a) and mechanically pulverized; (b) $MmNi_{4.6}Fe_{0.4}$ alloys and the inset picture focus on broadening of full width at half maximum (FWHM). reproduced from [61], with permission from Elsevier, 2004.

Table 3. Hydrogenation properties of metal alloys synthesized by mechanical alloying.

Mg-based alloys						
Alloy type	Alloy material	Milling conditions (rotation speed and milling time)	Particle size distribution, μm	Hydriding kinetics, min^{-1}	Hydrogen capacity, wt. %	References
As-cast alloy	Mg	–	48–70	1.4×10^{-3}	7.66	[57]
As-milled alloys	Mg	500 rpm for 120 min	<0.05	0.04	4.98	[37]
	Mg-10FeTiO ₃	500 rpm for 120 min	<0.05	0.07	2.71	
	Mg-10FeTiO ₃ -5MWCNT	500 rpm for 120 min	<0.05	0.31	5.22	
	Mg-10(FeV)	500 rpm, for 300 min	0.001–0.01	0.02	6.96	[47]
	Mg-10(FeV)-5MWCNT	500 rpm, for 300 min	~0.01	0.02	6.69	
	Mg-0.5Pd	500 rpm, for 360 min	0.05–0.1	0.04	5.13	[48]
	Mg-5Pd	500 rpm, for 360 min	<0.01	0.02	5.56	
AB ₂ -type alloys						
Alloy type	Alloy material	Milling conditions (rotation speed and milling time)	Particle size distribution, μm	Hydriding kinetics, min^{-1}	Hydrogen capacity, wt. %	References
As-cast alloy	Ti _{0.5} Zr _{0.5} MnCr	–	15–29	0.04	1.79	[65]
As-milled alloys	Ti _{0.5} Zr _{0.5} MnCr	Milled for 5 min	~8	0.13	1.82	
		Milled for 30 min	3–6	0.05	1.65	
		Milled for 60 min	0.5–1.7	0.06	1.15	
As-milled alloys	Mg(Ni _{0.75} Mn _{0.25}) ₂	350 rpm for 600 min	<10	0.25	0.43	[66]
	Mg(Ni _{0.1} Mn _{0.9}) ₂	350 rpm for 600 min		0.14	0.93	
	MgMn ₂	350 rpm for 600 min		0.1	1.21	
AB ₅ -type alloys						
Alloy type	Alloy material	Milling conditions (rotation speed and milling time)	Particle size distribution, μm	Hydriding kinetics, min^{-1}	Hydrogen capacity, wt. %	References
As-cast alloy	MmNi ₅	–	5–50	0.24	1.20	[67]
As-milled alloy	MmNi ₅	200 rpm for 180 min	1–2	0.28	1.42	
As-cast alloy	MnNi _{4.6} Fe _{0.4}	–	~9.58	–	1.50	[62]
As-milled alloys	MnNi _{4.6} Fe _{0.4}	200 rpm for 10 min	–	–	2.00	
		200 rpm for 30 min	~1.62	–	1.82	
		300 rpm for 10 min	–	–	1.91	
		300 rpm for 30 min	–	–	1.21	

To be more accurate, not only particle size gives precise measurement of hydrogen uptake capacity by a material, but it also provides the nature of agglomeration, as well as homogeneity of the particles [62]. Short milling process yields non-homogeneous microstructural (wide distribution of nano-crystallite sizes and amorphous phase) and morphological alloy powders [25]. On the other hand, Parker et al. [35] recommends defects, fractures and porosity as faster absorption kinetics agents. However, it is very challenging to fully release hydrogen from a porous and fractured material. Figure 6 depicts SEM images of un-milled MmNi₅ alloy and those of MmNi₅ milled with different transition metals at concentration of 2.0 wt. %. for un-milled alloy, its structure lacks strain and consists of very large particles, and thus, hydrogen diffusion is difficult for such material [67].

In contrast to MnNi_{4.6}Fe_{0.4} alloy, neither covalent nor ionic bonding is expected between the bulk alloy MmNi₅ and the added transition metals (Co, Ni, Mn and Fe), since there was no substitution or melting during mechanical milling, thus, a physical attachment was involved [67]. As a result, the extent to which the particles of each alloy crush and become reduced in size during milling depends largely on ductility and hardness of the transition metal used. According to Mohs scale of metal hardness, Mn has Mohs hardness of 6, followed by Co with hardness of 5 and the last two are Fe and Ni both with hardness of 4.5 and 4, respectively [68]. Therefore, during ball milling, it is difficult to fracture and form finer powders with Mn particles than with Ni particles.

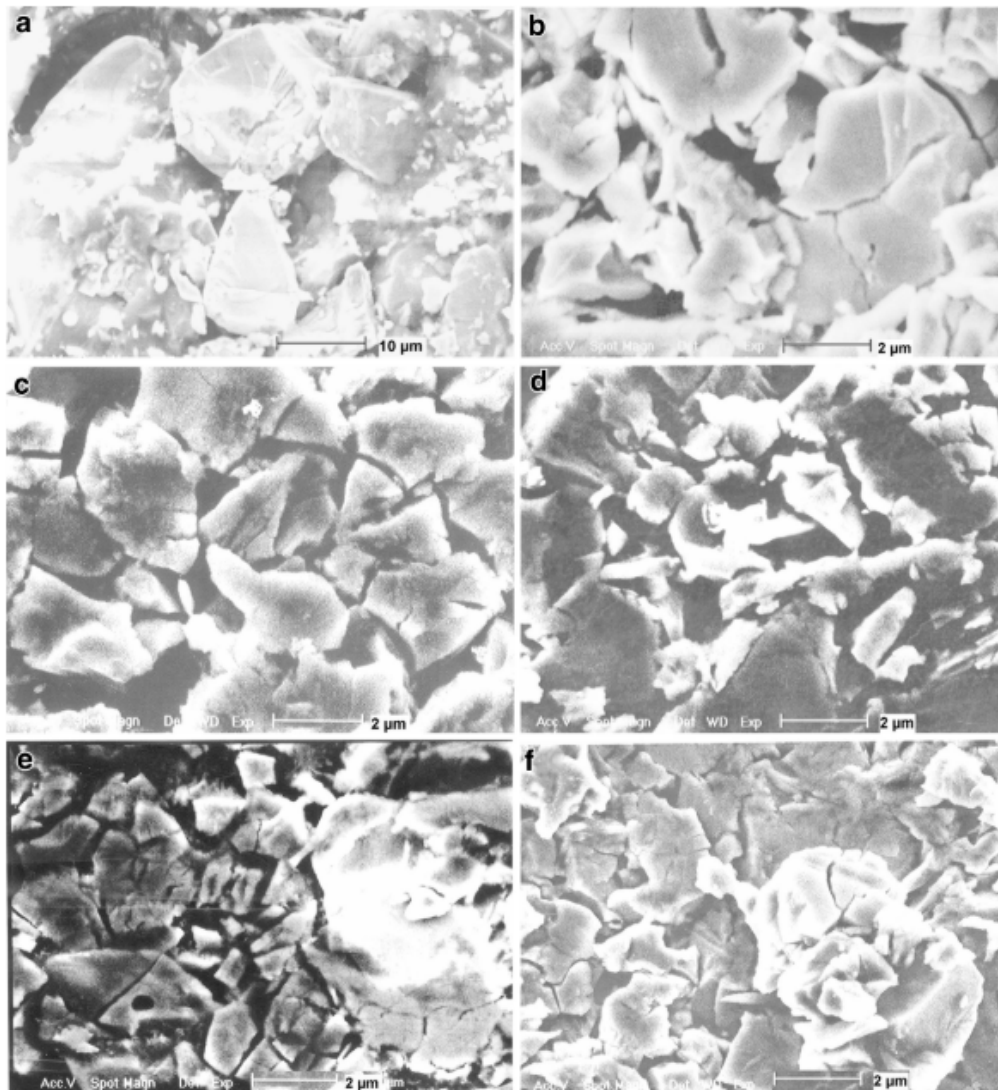


Figure 6. SEM micrographs of (a) bulk $MmNi_5$ alloy; (b) ball-milled $MmNi_5$ alloy; (c) $MmNi_5$ alloy ball-milled with Co; (d) Ni; (e) Mn and (f) Fe transition metals at concentration of 2.0 wt. %, obtained from [60].

3.3.2. Hydrogen Absorption Behaviour of Mechanically Alloyed AB_5 -Type Alloys

These metal hydride alloys are typified by $LaNi_5$ and they can be easily activated for hydrogen absorption [69]. A reaction between these alloys and hydrogen at a room temperature and pressure above equilibrium plateau pressure results in a ternary metal hydride [69]. Of 37 voids available within $LaNi_5$ lattice structure, only 6 voids are occupied by hydrogen atoms to form $LaNi_5H_6$ ternary hydride [70]. It is notable that the hysteresis effect in AB_5 -type alloy is relatively small as compared to other low temperature systems with a large and distinct miscibility gap [59]. Mechanical alloying has also been employed to synthesize AB_5 alloys [25,62,67,71]. For example, $MmNi_5$ material mechanically alloyed at 200 rpm for milling time of 180 min exhibits faster hydrogenation kinetics as compared to arc-melted $MmNi_5$ material [67]. Furthermore, Figure 7a,b present the absorption and desorption kinetic curves of $MmNi_5$ alloy ball-milled with transition metals at concentration of 2.0 wt. %, respectively, showing reversible hydrogen absorption and desorption between 1.0 to 1.6 wt. % [67]. Singh and co-workers [62] observed that longer milling of $MnNi_{4.6}Fe_{0.4}$ alloy material improved hydriding kinetics, but this elevated kinetics behaviour comes at a cost of maximum uptake capacity as it deteriorated with increasing milling time. On the same note, an increase in rotation

speed from 200 rpm to 300 rpm at constant milling time resulted in a reduction of hydrogen capacity. Similar trend was observed by Ares and co-workers [25] and they summarized that the trend is a result of extra hydrogen-trapping sites in amorphous domains, exhibited by short-milled alloys. For LaNi_5 alloy, it is reported that ball-milling convert a part of LaNi_5 to a non-absorbing state and as a result poor hydrogen uptake capacity is observed [71]. It was seen that there is quite a number of published work found in the literature for mechanical alloying of AB_5 -type alloys [62,67]. However, understanding the general extent to which mechanical alloying enhance the ability of these type of alloys to absorb hydrogen, as compared to their traditionally or arc-melted counterparts is still a gap. Firstly, to our knowledge no proper measurements of the hydrogen sticking or diffusion probabilities on either un-milled or milled AB_5 -type particles have been documented. The second issue is that mechanical alloying tempers with several physical properties that are vital for hydrogen sorption performance; these include expansion of the unit cell volume, strain and homogeneity of particles, particle size distribution, distance between adjacent voids and several more.

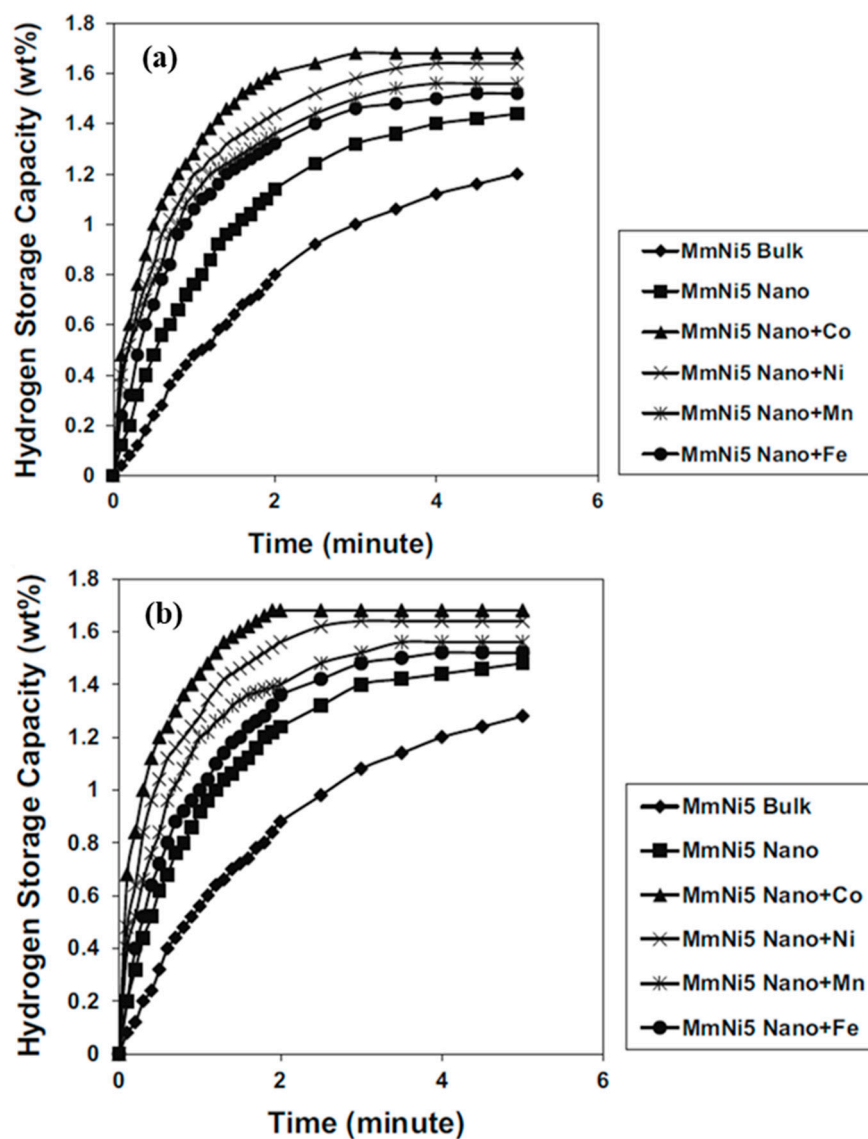


Figure 7. (a) Absorption kinetic curves of MmNi_5 alloy ball-milled with transition metals at concentration of 2.0 wt. %, and (b) Desorption kinetic curves of MmNi_5 alloy ball-milled with transition metals at concentration of 2.0 wt. %. Reprinted from [67].

3.4. AB₂-Type Alloys

3.4.1. Structural Characteristics of Mechanically Milled AB₂-Type Alloys

In the AB₂ Laves phase alloy, metal A is usually Ti or Zr, and metal B is another transition metal including V, Cr or Mn. These alloys crystallize in Lave phase structures [72,73]. Three types of laves phases; namely: hexagonal C14 phase (MgZn₂), hexagonal C36 phase (MgNi₂) and cubic C15 phase (MgCu₂) represent AB₂- type alloys [72]. In comparison, hydrogenation performance of hexagonal C36 phase has been reported to be poor [73], and it is not reviewed here. C15 and C14 phases (corresponding to atomic ratio of $R_A/R_B = 1.225$) have shown better performance as hydrogen absorbents [73]. Based on their structural stability, which is dependent on the atomic ratio, electronegativity and valence of the elements used [74,75], hexagonal C14 ZrCr₂ Laves phases are more stable compared to cubic C15 [76].

Figure 8 represents example of powder diffraction patterns for C14 Laves phase type alloys. As seen with Mg-based and AB₅-type alloys discussed earlier in this review, longer milling periods results in reduction of crystallite size and particle size. Furthermore, several other factors such as disappearance of peaks (between $2\theta \approx 48$ and 100 in Figure 8), as well as peak broadening occur. To some extent, intense change of these factors may result in deterioration of hydrogen performance.

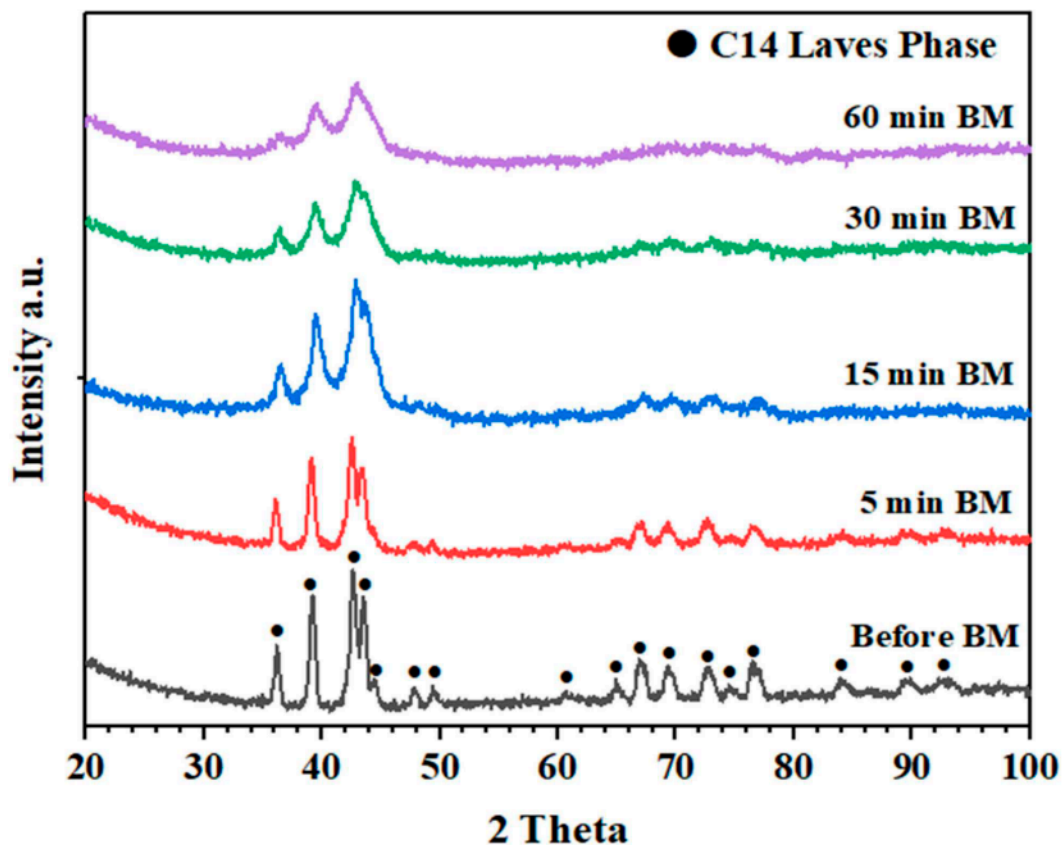


Figure 8. Powder diffraction patterns of alloy Ti_{0.5}Zr_{0.5}MnCr before and after 5, 15, 30 and 60 min of ball milling, reproduced from [65], with permission from Elsevier, 2019.

3.4.2. Hydrogen Absorption Behaviour of Mechanically Alloyed AB₂-Type Alloys

The reported hydrogen storage of AB₂-type alloys is nearly 2 wt. %, with low hysteresis [75]. But binary AB₂-type alloys prepared by equilibrium techniques suffer from poor surface activity and poisoning intolerance [77]. As a result, efforts through synthesizing AB₂ alloys utilizing non-equilibrium techniques such as mechanical alloying have been exploited [66]. For example, Ti_{0.5}Zr_{0.5}MnCr material prepared through mechanical alloying for a milling period of 5 min was reported to exhibit larger

hydrogen absorption capacity compared to as-cast $\text{Ti}_{0.5}\text{Zr}_{0.5}\text{MnCr}$ and materials milled much longer (Table 3 and Figure 9) [65].

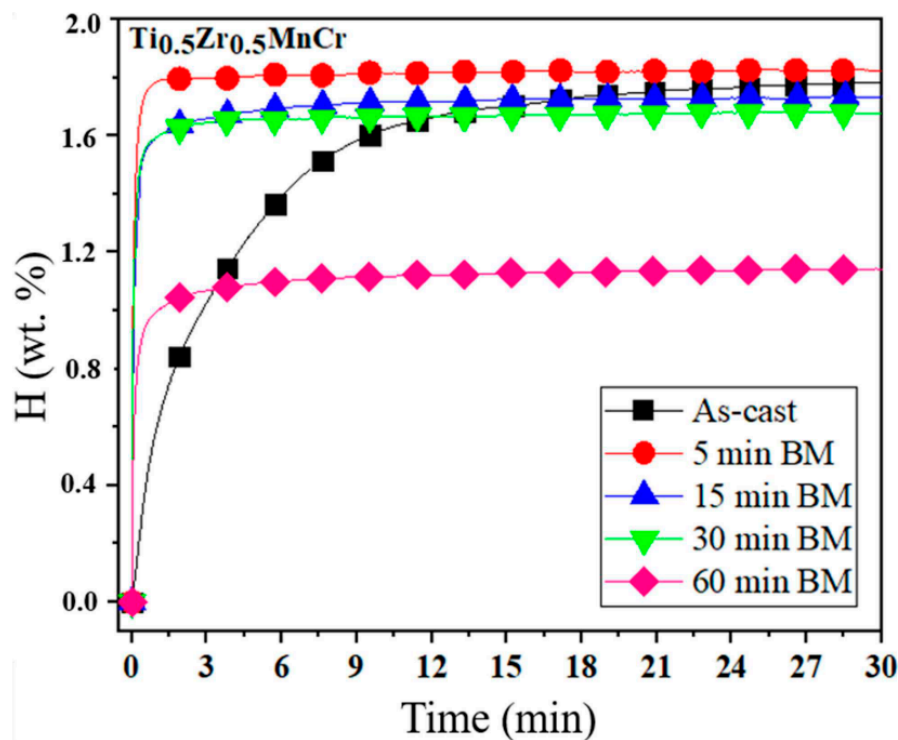


Figure 9. Hydrogenation kinetics of $\text{Ti}_{0.5}\text{Zr}_{0.5}\text{MnCr}$ alloys before and after ball milling for 5, 15, 30 and 60 min, reproduced from [58], with permission from Elsevier, 2019.

However, those that are milled longer than 5 min exhibit faster hydriding kinetics and poor hydrogen absorption capacity compared to as-cast alloy [65]. Based on the literature data contained in this document, we understand that fractured fine, smaller particle sizes and amorphous nature, which are obtained through milling time above 25 min favour faster hydrogenation kinetics. Whereas combination of large to moderate particles and nano-crystalline structure, obtained during short milling time of less than 10 min favours large hydrogen absorption capacity.

3.5. Comparison between Hydriding Kinetics of Materials Prepared by MA with Other Techniques

Apart from mechanical alloying, melt spinning and spark plasma sintering techniques are also prevailing synthesis methods and thus we opted to make some comparisons between these three methods. Melt-spinning technique is a useful method that is used to change structures of as-cast alloys to amorphous structure. This method improves the amorphous nature of materials by reducing their grain size [44]. The only problem related to this method is the poor cycle stability of the melt-spun alloys, due to the disappearing of the metastable structures generated by melt-spinning [78]. Another attracting technique is spark plasma sintering (SPS), due to its ability to easily synthesize metal powders, with different melting temperatures within just 5–10 min [79]. This technique involves generation of spark plasma through direct pulse current and working concurrently with a uniaxial pressure. Sintering takes place at low temperatures in a small period of time and this makes the alloys to have low porosity [80]. SPS offers numerous favourable advantages over customary sintering procedures such as atmospheric furnace. For instance, the heating rate around 1273 K per min can be accomplished [79]. Further focal points are the lower sintering temperature, short holding time, no need of pre-compaction and shorter sintering time results in the likelihood to sinter nanometric powder to near theoretical density [81]. Although this technique produces alloys with high purity

surfaces, it is known that the hydriding kinetics of composites, prepared by SPS, is greatly improved only when hydrogen absorption is conducted at high temperatures (573 K) [79].

Huang et al. [82] reported that alloys with amorphous surfaces absorb hydrogen faster compared to their crystalline counterparts. Schwarz and Johnson [83] recommended that two conditions should be fulfilled for an amorphous phase to form from a mixed elemental powder blend. The first condition is that the metals involved must have a vast negative heat of blending in the liquid state. According to a study conducted by Termsuksawad et al. [84], metals that have large negative heat of mixing exhibited a complete amorphous phase, while those with smaller negative heat displayed partial amorphous nature. Second, the condition is that diffusion rates of such metal systems must differ greatly. Metal alloy materials with nano-crystalline and/or amorphous phases are easily obtainable through several preparation techniques, including mechanical milling, spark plasma sintering and melt spinning [85,86]. There are numerous published papers supporting the above statement, and we combined some of those findings in Table 4. All the as-milled, as-spun and sintered alloy materials in Table 4 are reported to exhibit amorphous phases, and they are compared with their as-cast crystalline counterparts. According to the table, mechanical alloying of as-cast materials usually has a negative impact on the maximum hydrogen absorption capacity as all materials showed drastic decrease in their respective hydrogen content, except for $\text{Ti}_{0.5}\text{Zr}_{0.5}\text{MnCr}$ alloy. Similar to other authors, Khajavi et al. [65] rationalized a loss in hydrogen capacity by deducing that milling process decreases the crystallite size, resulting in peak broadening. Nonetheless, milling significantly enhanced the absorption kinetics, and this is indicated by exceptional rate constants associated with all the as-milled counterparts in Table 4. Almost all the rate constants presented in the table were estimated from kinetic curves using chemisorption model [65] as shown by Equation (4),

$$\alpha = kt \quad (4)$$

where α is the reacted fraction, t is hydrogenation time and k is rate constant. Metastable alloys (as amorphous, nano-crystalline, quasicrystalline, polycrystalline) can be prepared through melt spinning technique, since it allows quick quenching of melted metals. Most as-spun materials reported in this review have amorphous (examples being $\text{Mg}_{11}\text{Y}_2\text{Ni}_2$ and $\text{Mg}_3\text{LaNi}_{0.1}$) and nano-crystalline phases (examples being Mg-10Ni-2Mn and $\text{Mg}_2\text{Ni}_{0.9}\text{Co}_{0.1}$). On a contrary to mechanical alloying, melt spinning technique enhances both the hydrogen storage capacity and the kinetics (Table 4). The speedy hydrogenation kinetics for as-spun materials can be related to fine particle size and the crystal defects shaped as a result of rapid solidification, which facilitates swift nucleation and diffusion of hydrogen [23]. The enormous quantity of interfaces and grain boundaries created within the as-spun alloy offers easy access for hydrogen diffusion and facilitate easy absorption of hydrogen [23]. Another interesting technique featured in this review is spark plasma sintering. In the same way as MA and melt spinning, SPS-synthesized alloy materials exhibit an amorphous/nanocrystallite phase [87,88]. The absorption kinetics and capacity of sintered materials are affected by the amount (percentage), the type of material, and sintering conditions (temperature and pressure) used for SPS process. For example, hydrogen content of metallic Mg was reduced extremely from 7.26 wt. % to 2.52 wt. % upon blending with 77% $\text{V}_{77.8}\text{Zr}_{7.4}\text{Ti}_{7.4}\text{Ni}_{7.4}$ through SPS while hydrogen content of $\text{V}_{35}(\text{Ti,Cr})_{65}$ sintered with ZrMn_2 remained almost the same [87,88]. Interestingly, the rate constants of sintered alloy materials in Table 4 are better than those of as-cast materials. This is a clear indication that the SPS method has a positive effect on hydrogen absorption kinetics. Thus, it can be seen that all these three techniques are good candidates for improvement of hydrogen absorption kinetics, but alloys prepared using SPS technique in most cases have low hydrogen capacity. Hence, we take a further comparison between the prevailing techniques—MA and melt spinning.

Table 4. Comparison of hydrogenation kinetics and capacity of as-cast alloys and those prepared by MA, SPS and melt spinning.

Mechanical Alloying/Milling						
Material	Rate constant (min ⁻¹)		Hydrogen absorption capacity (wt. %)		Conditions	References
	As-cast	As-milled	As-cast	As-milled		
Metal alloy material	As-cast	As-milled	As-cast	As-milled		
Mg ₂ Ni	0.06	0.15	2.91	2.60	473 K, 1.0 MPa	[66]
TiFe+4 wt. % Zr (60 min milling)	9.0 × 10 ⁻³	0.01	1.62	1.27	273 K, 4.5 MPa	[89]
TiFe+4 wt. % Zr (5 min milling)	9.0 × 10 ⁻³	8.5 × 10 ⁻³	1.62	1.41	273 K, 4.5 MPa	[89]
Ti _{0.5} Zr _{0.5} MnCr (60 min milling)	0.04	0.05	1.75	1.05	273 K, 2.0 MPa	[65]
Ti _{0.5} Zr _{0.5} MnCr (5 min milling)	0.04	0.05	1.75	1.82	273 K, 2.0 MPa	[65]
Melt-spinning technique						
Material	Rate constant (min ⁻¹)		Hydrogen absorption capacity (wt. %)		Conditions	References
	As-cast	Melt-spun	As-cast	Melt-spun		
Metal alloy material	As-cast	Melt-spun	As-cast	Melt-spun		
Mg ₁₁ Y ₂ Ni ₂	0.90	0.52	3.61	3.89	523 K, 3.0 MPa	[90]
Mg ₃ LaNi _{0.1}	0.25	0.60	2.73	2.90	573 K, 4.0 MPa	[24]
Mg-10Ni-2Mn	0.01	0.02	4.67	5.09	598 K, 1.0 MPa	[23]
Mg ₂ Ni _{0.9} Co _{0.1}	9.0 × 10 ⁻³	0.02	2.38	3.00	473 K, 1.5 MPa	[91]
Spark plasma sintering						
Material	Rate constant (min ⁻¹)		Hydrogen absorption capacity (wt. %)		Conditions	References
	As-cast	Sintered	As-cast	Sintered		
Metal alloy material	As-cast	Sintered	As-cast	Sintered		
Mg sintered with 77% V _{77.8} Zr _{7.4} Ti _{7.4} Ni _{7.4}	1.7 × 10 ⁻³	6.7 × 10 ⁻³	7.26	2.52	573 K, 3.0 MPa	[87]
V ₃₅ (Ti,Cr) ₆₅ sintered with ZrMn ₂	0.01	0.04	2.86	2.89	303 K, 0.6 MPa	[88]
Mg sintered with 30% ZrMn ₂	1.7 × 10 ⁻³	3.3 × 10 ⁻³	7.26	6.34	573 K, 3.0 MPa	[87]

Zhang et al [44] and Wu et al [92] made some efforts to prepare and compare structures and hydrogenation behaviour of as-milled and as-spun alloy materials. Their findings are summarized in Table 5. From the table, it can be seen that the hydrogen absorption capacity of Mg-10Ni-2Mm alloy is favoured by melt spinning technique as larger amount of hydrogen was stored by the material prepared through this technique than that prepared using mechanical alloying. However, YMg₁₁Ni in Table 5 showed a different trend. The rate constants of materials prepared by mechanical alloying are better than those of materials synthesized by melt spinning technique. This indicates that mechanical alloying plays a significant influence on increasing the hydrogenation kinetics of the alloys as compared to melt spinning.

Table 5. Comparison between kinetics and hydrogen content of as-milled and as-spun techniques.

Material	Rate constant, min ⁻¹		Absorption Capacity, wt. %		Conditions	References
	As-milled	As-spun	As-milled	As-spun		
Mg–10Ni–2Mm	0.04	0.01	3.21	4.22	573 K, 2.0 MPa	[92]
YMg ₁₁ Ni	0.05	0.03	4.72	4.07	593 K, 3.0 MPa	[44]

Hydrogenation of metal alloys is usually governed by three steps, namely (i) dissociation of hydrogen molecules into atomic hydrogen, (ii) the penetration of atomic hydrogen through grain boundaries, and (iii) the binding of atomic hydrogen on the metal, transforming into metal hydride [44]. The rate-determining step of the as-milled alloy is most likely ascribed to the ball milling rendering the second step, i.e., the penetration of atomic hydrogen through grain boundaries. The milling of as-cast alloys during mechanical alloying results in reduction of particle size and increment of high surface-to-volume ratio of alloy particles [93]. Due to these two changes, the distance for atomic hydrogen penetrating through the material is extremely reduced, which facilitates absorption greatly.

3.6. Surface Modification of Ball Milled Metal Alloys

Better and improved hydrogenation kinetics are achieved by nano-crystalline and/or amorphous metal alloys synthesized by mechanical alloying, but such materials still encounter several limitations, including impurity interactions, which include poisoning of the metal by impure gases such as carbon monoxide, sulphur and carbon dioxide; disproportionation during absorption/desorption cycling; retardation; innocuous and difficulty of initial activation [94]. These shortcomings result in rapid loss of hydrogen capacity with cycling, caused by impurities strongly or irreversibly absorbed on the surface active sites, and loss in absorption kinetics due to surface blanketing [95]. To overcome the above-mentioned problem, nano-structuring of ball milled materials and surface modification technology can be employed before hydrogen sorption can take place [96]. Surface modification involves the formation of a protective layer on the surface of metal alloy, thus preventing oxide-containing film to form. The most common surface modification technologies include fluorination, potassium borohydride, Ni-weak acid, ion implantation, hydrochloric (HCl) acid, platinum group metals (PGMs) decomposition and Y₃O₂ deposition. Yeung et al. [97] reported that the surface modification techniques PGMs deposition is the most attractive technology due to its ability to simultaneously prevent deactivation by guarding the catalytically active sites on the surface of bulk material against and enhance the hydriding kinetics during hydrogen absorption [97–100]. Moreover, this technique does not only enhance the hydriding rate, but also the absorption capacity of the alloys [99]. In particular, palladium is capable of catalyzing hydrogen sorption reactions, promoting easy activation, and improving poisoning tolerance. It has high hydrogen affinity and it is impermeable to larger molecules such as CO₂ and sulphur [82]. Figure 10a–c show different mechanisms of hydrogen dissociation on the surface of Pd-treated AB₅-type alloys [100]. During the hydrogen spillover mechanism hydrogen molecules are dissociated into hydrogen atoms on the surface of palladium, which then spillover to the active sites of the bulk alloy [98]. Pd thin film on the surface of AB₅ alloy dissociates hydrogen molecules and allows the resulting hydrogen atoms to pass through the film as they diffuse into the bulk alloy. However, this technique is costly as huge amount of Pd is utilized [99].

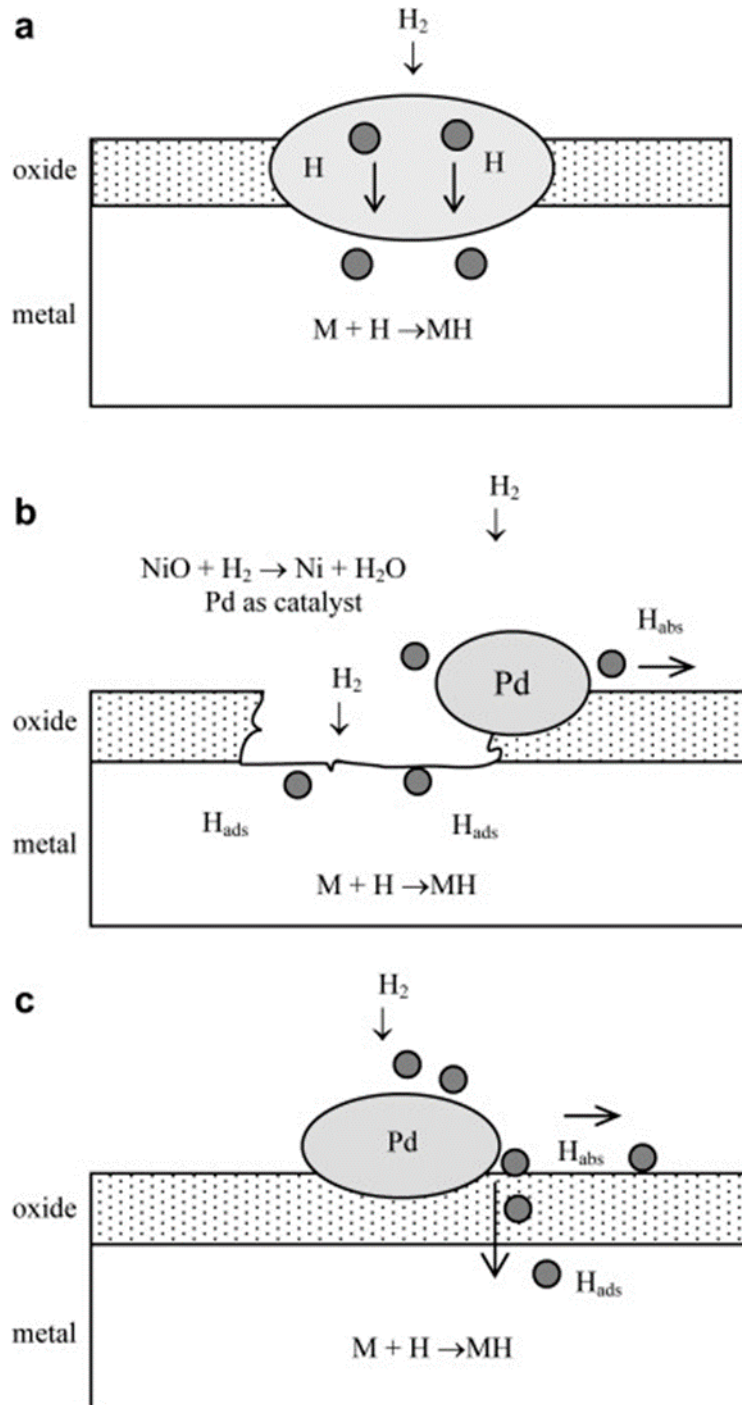


Figure 10. Different mechanisms of hydrogen dissociation on the surface of Pd-treated alloy material; (a) hydrogen diffusion through Pd window, (b) hydrogen spillover with oxide layer being reduced by spilt hydrogen from palladium, and (c) hydrogen spillover with hydrogen atoms diffusing through the oxide layer, reproduced from [100], with permission from Elsevier, 2009.

Moreover, PGM-treated materials also exhibit the power to absorb hydrogen at low temperature, without the activation step prior to absorption, and enhanced kinetics of hydrogen sorption processes [101]. This method is extremely active towards dissociative hydrogen chemisorption and permeable for hydrogen atoms; enabling hydrogen to rapidly absorb into the bulk material while still maintaining the hydrogenation activity even after exposure to the impurities inhibiting hydrogen sorption [102]. The properties being improved include surface catalytic activity, specific

surface area layer, activation characteristics, as well as protective nature of the complexes against poisoning materials, such as sulphur, water vapour and carbon oxides [82].

Davids et al. [103] exploited hydrogenation behaviour of ball-milled TiFe alloy surface modified using a metal-organic chemical vapour deposition technique (MOCVD), by the thermal decomposition of palladium (II) acetylacetonate ($\text{Pd}[\text{acac}]_2$), mixed with the powder of the parent alloy. The authors reported that alloy materials containing 0.5% Pd have better hydrogenation behaviour than materials containing 1% Pd. The same trend in deterioration of hydrogenation performance, with an increase in Pd content, was observed by Pasquini and co-workers [104] who varied Pd content (corresponding to 4, 8 and 13 wt. %) on the surface of Mg metal. The observations are due to the theory that large amount of metal deposits on the surface of TiFe alloy and Mg metal results in slow penetration of hydrogen over a given period [104], as a result of fracture and defect blockage of the parent alloy material, which are usually formed during ball milling. Doyle et al. [105] recommended that the total weight of PGMs during surface modification of metal hydride-forming alloy should be in trace amounts (≤ 0.1 wt. %) to avoid losses in hydrogenation behaviour. Another interesting study in literature was conducted by Modibane et al. [106] in which the authors carried out ball milling of AB_5 -type materials out using a FRITSCH Pulverisette planetary mill and subsequently deposited Pd nanoparticles using autocatalytic Pd deposition technique. Upon ball milling of the parent alloy (Figure 11a), porous agglomerates of micro-size particles (Figure 11b,c) were obtained due to blending and grinding of parent particles. Porous particles are fancied by Parker et al. [35] for enhancement of absorption kinetics. Palladium nanoparticles, which showed discontinuous nature and near-spherical shape, partially cover the AB_5 materials (Figure 11d–f) and are responsible for dissociation of hydrogen molecules [106].

Table 6 reveals some of reported literature on surface modified metal alloys synthesized through mechanical alloying. Surface modification techniques herein are based on PGMs deposition and co-deposition. All surface modified alloys exhibit better hydrogenation kinetics as compared to their as-milled counterparts. Variations arise when comparing the hydrogen capacities. For instance, Pt deposition on as-milled $\text{La}_{0.9}\text{Pr}_{0.05}\text{Nd}_{0.05}\text{Al}_{0.3}\text{Mn}_{0.4}\text{Co}_{0.65}\text{Ni}_{3.5}$ alloy results in increase of capacity, while Ru deposition on the same alloy lowers the hydrogen capacity. This is attributed to poor or little hydrogen affinity associated with Ru.

Table 6. Hydrogenation properties of surface modified metal alloys prepared by mechanical alloying.

Alloy Type	Metal Alloy	Rate Constant, min^{-1}	Hydrogen Capacity, wt. %	Hydrogenation Conditions	References
As-milled	LaNi_5	0.04	5.30	313 K, 1.5 MPa	[28]
Pd deposition	Pd-LaNi_5	2.38	5.18	313 K, 1.5 MPa	
As-milled	Mg_2Ni	0.06	3.55	673 K, 2.0 MPa	[28]
Pd deposition	$\text{Pd-Mg}_2\text{Ni}$	0.59	2.64	573 K, 2.0 MPa	
As-milled	$\text{LaNi}_{4.25}\text{Al}_{0.75}$	4.8×10^{-1}	3.21	293 K, 1.5 MPa	[107]
Pd deposition	$\text{Pd-LaNi}_{4.25}\text{Al}_{0.75}$	1.33	3.89	293 K, 1.5 MPa	
As-milled	$\text{La}_{0.9}\text{Pr}_{0.05}\text{Nd}_{0.05}\text{Al}_{0.3}\text{Mn}_{0.4}\text{Co}_{0.65}\text{Ni}_{3.5}$	2.4×10^{-3}	0.45	293 K, 0.5 MPa	[108]
Pt deposition	$\text{Pt-La}_{0.9}\text{Pr}_{0.05}\text{Nd}_{0.05}\text{Al}_{0.3}\text{Mn}_{0.4}\text{Co}_{0.65}\text{Ni}_{3.5}$	4.5×10^{-2}	0.83	298 K, 0.1 MPa	
Ru deposition	$\text{Ru-La}_{0.9}\text{Pr}_{0.05}\text{Nd}_{0.05}\text{Al}_{0.3}\text{Mn}_{0.4}\text{Co}_{0.65}\text{Ni}_{3.5}$	3.3×10^{-2}	0.34	298 K, 0.1 MPa	
Pt-Ru co-deposition	$\text{Pt-Ru-La}_{0.9}\text{Pr}_{0.05}\text{Nd}_{0.05}\text{Al}_{0.3}\text{Mn}_{0.4}\text{Co}_{0.65}\text{Ni}_{3.5}$	2.9×10^{-2}	0.79	298 K, 0.1 MPa	[101]
As-milled	$\text{La}_{0.40}\text{Ce}_{0.48}(\text{Nd,Pr})_{0.16}\text{Ni}_{3.34}\text{Co}_{0.64}\text{Al}_{0.63}\text{Mn}_{0.58}$	1.6×10^{-4}	1.24	293 K, 0.5 MPa	
Pd deposition	$\text{Pd-La}_{0.40}\text{Ce}_{0.48}(\text{Nd,Pr})_{0.16}\text{Ni}_{3.34}\text{Co}_{0.64}\text{Al}_{0.63}\text{Mn}_{0.58}$	6.2×10^{-4}	2.75	293 K, 0.5 MPa	
Pd-Ni co-deposition	$\text{Pd-Ni-La}_{0.40}\text{Ce}_{0.48}(\text{Nd,Pr})_{0.16}\text{Ni}_{3.34}\text{Co}_{0.64}\text{Al}_{0.63}\text{Mn}_{0.58}$	1.1×10^{-3}	3.60	293 K, 0.5 MPa	

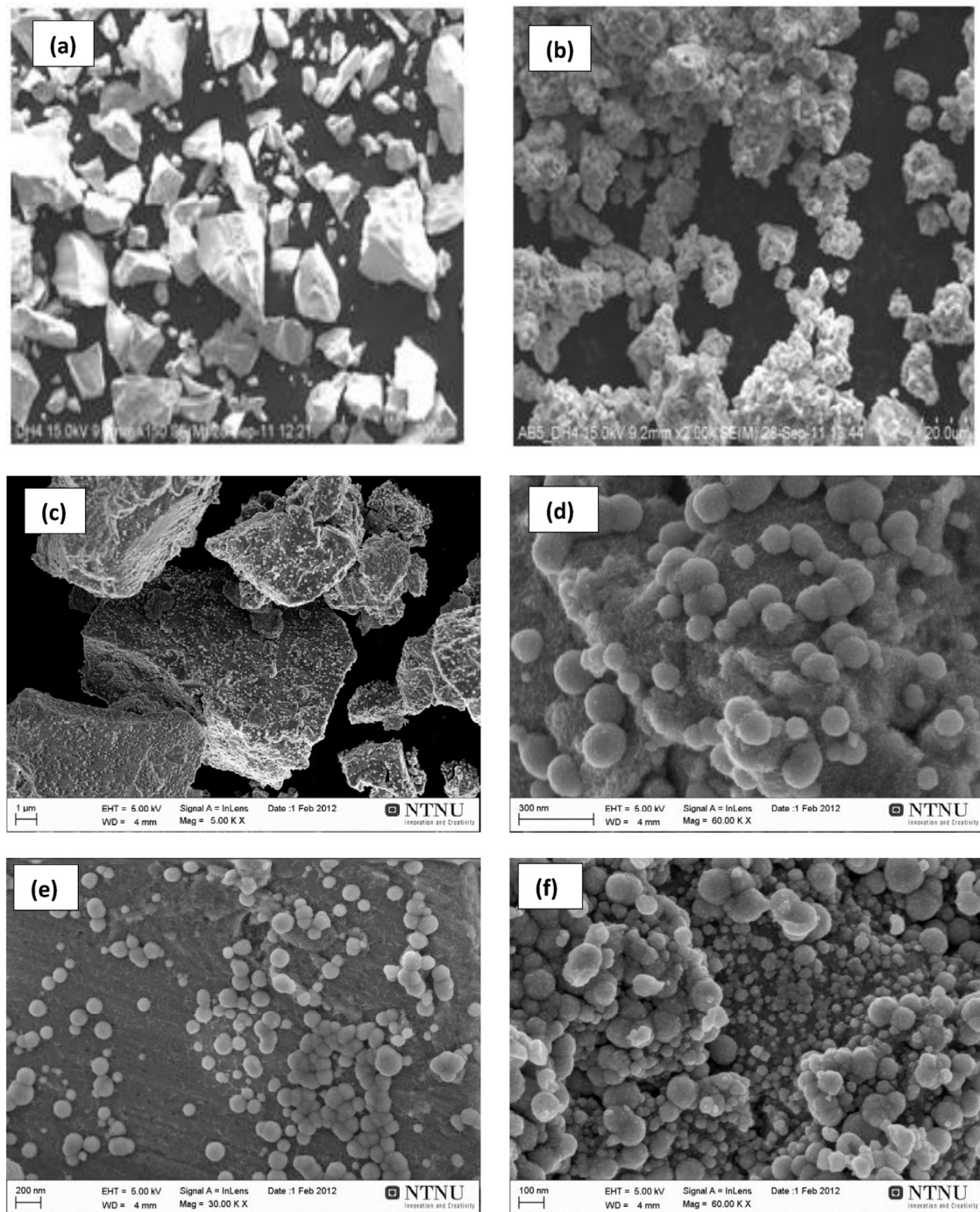


Figure 11. Low-((a,b), Hitachi X-650 EM) and high-resolution ((c–f), Zeiss Ultra) SEM images of raw AB5 alloy (a), the alloy ball milled without Pd black (b), and the alloy ball milled with Pd black after autocatalytic Pd deposition at different magnifications (c–f), reproduced from [106], with permission from Elsevier, 2018.

4. Conclusions

Hydrogenation kinetics and storage in solid state materials is a major concern in developing an up-and-coming hydrogen technology and economy. The present work reviews some challenges regarding the hydride-forming alloys, particularly their hydriding kinetics and capacity. In this regard, developments on hydrogenation performances of metal alloys, prepared by the mechanical alloying technique, were discussed. Moreover, this technique was compared with other preparation

techniques, such as spark plasma sintering and melt spinning. The work is carried out in an attempt to facilitate suitable alloy preparation technique that can extensively improve the hydrogenation kinetics of different alloy materials. Although, much attention has been given to the techniques that are discussed in this work, with the aim of minimizing dehydrogenation temperature, enhancing the kinetics and poisoning-tolerance of different alloys, further research is needed. The collected literature data reveal encouraging improvements in terms of hydrogen storage kinetics through mechanical alloying. In the light of the achievements, through the combination of mechanical alloying and melt spinning techniques there is high potential in developing better metal hydride materials with high hydriding kinetics. Mechanically alloyed materials still suffer from cycling stability; they are prone to oxide layers formation, which hinders rapid absorption of hydrogen; and they also exhibit poisonous-intolerance. As a result, we further reviewed different surface modification techniques that can overcome these drawbacks. Surface modification of mechanically alloyed materials was overlooked at and it was seen that it promotes hydrogen storage kinetics by forming a protective layer on the surface of bulk alloy, thereby preventing the formation of oxide layer. Moreover, surface modification through deposition of PGMs on the surface of alloy materials stimulates poisonous tolerance of parent alloys.

Author Contributions: Conceptualization, K.D.M., and M.V.L.; funding acquisition, K.D.M. and M.J.H.; project administration, K.D.M.; Supervision, K.D.M., and M.V.L.; writing—original draft, T.R.S., T.C.M., M.W.D., K.D.M., M.J.H. and M.V.L. All authors have read and agreed to the published version of the manuscript.

Funding: This research was supported by the National Research Foundation under Thuthuka program (UIDs. 117727 and 118113), University of Limpopo (Research Development Grants R202 and R232) and Sasol Inzalo Foundation, South Africa.

Conflicts of Interest: The authors declare no conflict of interest.

References

1. Andreas, R. Hydrogen storage methods. *Naturwissenschaften* **2004**, *91*, 157–172.
2. Schlapbach, L.; Züttel, A. Hydrogen-storage materials for mobile applications. *Mater. Sustain. Energy* **2011**, *414*, 265–270.
3. Berlouis, L.E.A.; Cabrera, E.; Hall, P.J. Thermal analysis investigation of hydriding properties of nanocrystalline Mg–Ni–and Mg–Fe-based alloys prepared by high-energy ball milling. *J. Alloys Compd.* **2000**, *305*, 82–89. [[CrossRef](#)]
4. Sakintuna, B.; Lamari-darkrim, F.; Hirscher, M. Metal hydride materials for solid hydrogen storage: A review. *Int. J. Hydrog. Energy* **2007**, *32*, 1121–1140. [[CrossRef](#)]
5. Crivello, J.C.; Dam, B.; Yartys, V.A. Review of magnesium hydride-based materials: Development and optimisation. *Appl. Phys. A Mater. Sci. Process.* **2016**, *122*, 1–20. [[CrossRef](#)]
6. Liu, T.; Chen, C.; Qin, C.; Li, X. Improved hydrogen storage properties of Mg-based nanocomposite by addition of LaNi₅ nanoparticles. *Int. J. Hydrogen Energy* **2014**, *39*, 18273–18279. [[CrossRef](#)]
7. Yartys, V.A.; Lototskyy, M.V. An overview of hydrogen storage methods. In *Hydrogen Materials Science and Chemistry of Carbon Nanomaterials*; Springer: Dordrecht, The Netherland, 2004; pp. 75–104.
8. Berube, V.; Chen, G.; Dresselhaus, M.S. Impact of nanostructuring on the enthalpy of formation of metal hydrides. *Int. J. Hydrog. Energy* **2008**, *33*, 4122–4131. [[CrossRef](#)]
9. Pandey, S.K.; Srivastava, A.; Srivastava, O.N. Improvement in hydrogen storage capacity in LaNi₅ through substitution of Ni by Fe. *Int. J. Hydrog. Energy* **2007**, *32*, 2461–2465. [[CrossRef](#)]
10. Kazakov, A.N.; Dunikov, D.O.; Mitrokhin, S.V. AB₅-type intermetallic compounds for biohydrogen purification and storage. *Int. J. Hydrog. Energy* **2016**, *41*, 21774–21779. [[CrossRef](#)]
11. Takeda, H.; Kabutomori, T.; Ohnishi, K. Metal hydride air-conditioning. *Encycl. Life Support Syst.* **2009**, *2*, 249–263.
12. Davids, W.; Lototskyy, M.V.; Linkov, V. Chemical surface modification for the improvement of the hydrogenation kinetics and poisoning resistance of TiFe. *J. Alloys Compd.* **2011**, *509S*, S770–S774.
13. Semboshi, S.; Masahashi, N.; Hanada, S. Degradation of hydrogen absorbing capacity in cyclically hydrogenated TiMn₂. *Acta Metall. Sin.* **2001**, *49*, 927–935. [[CrossRef](#)]

14. Andreasen, A. Predicting formation enthalpies of metal hydrides. *Nature* **2001**, *414*, 353–358.
15. Chebab, S.; Abdellaoui, M.; Lacroche, M.; Paul-boncour, V. LaCaMgNi₉ synthesized by mechanical alloying: Structural and electrochemical characterization. *J. Tunis. Chem. Soc.* **2016**, *18*, 52–59.
16. Young, K. Increase in the Surface Catalytic Ability by Addition of Palladium in C14 Metal Hydride Alloy. *Batteries*. **2017**, *3*, 26. [[CrossRef](#)]
17. Zhang, Y.; Li, B.; Ren, H.; Ding, X.; Liu, X.; Chen, L. An investigation on hydrogen storage kinetics of nanocrystalline and amorphous Mg₂Ni_{1-x}Co_x (x = 0–0.4) alloy prepared by melt spinning. *J. Alloys Compd.* **2011**, *509*, 2808–2814. [[CrossRef](#)]
18. Simchi, H.; Kafrou, A.; Simchi, A. Synergetic effect of Ni and Nb₂O₅ on dehydrogenation properties of nanostructured MgH₂ synthesized by high-energy mechanical alloying. *Int. J. Hydrog. Energy* **2009**, *34*, 7724–7730. [[CrossRef](#)]
19. Suryanarayana, C. Mechanical alloying and milling. *Prog. Mater. Sci.* **2001**, *46*, 1–184. [[CrossRef](#)]
20. Suñol, J.J.; Fort, J. Materials developed by mechanical alloying and melt spinning. *Int. Rev. Phys.* **2008**, *2*, 31–35.
21. Scudino, S.; Sakaliyska, M.; Surreddi, K.B. Mechanical alloying and milling of Al-Mg alloys. *J. Alloys Compd.* **2009**, *483*, 2–7. [[CrossRef](#)]
22. Poondi, D.; Singh, J. Synthesis of metastable silver-nickel alloys by a novel laser-liquid-solid interaction technique. *J. Mater. Res.* **2000**, *35*, 2467–2476.
23. Xing, N.; Wu, Y.; Zhou, S. Improved hydrogenation-dehydrogenation characteristics of nanostructured melt-spun Mg-10Ni-2Mm alloy processed by rapid solidification. *Prog. Nat. Sci. Mater. Int.* **2010**, *20*, 49–53. [[CrossRef](#)]
24. Ouyang, L.Z.; Qin, F.X.; Zhu, M. The hydrogen storage behavior of Mg₃La and Mg₃LaNi_{0.1}. *Scr. Mater.* **2006**, *55*, 1075–1078. [[CrossRef](#)]
25. Ares, J.R.; Cuevas, F. Influence of thermal annealing on the hydrogenation properties of mechanically milled AB₅-type alloys. *Mater. Sci. Eng.* **2004**, *108*, 76–80. [[CrossRef](#)]
26. Guevara, L.; Welsh, R.; Atwater, M.A. Parametric Effects of Mechanical Alloying on Carbon Nanofiber Catalyst Production in the Ni-Cu System. *Metals (Basel)* **2018**, *8*, 286. [[CrossRef](#)]
27. Shang, C.X.; Bououdina, M.; Guo, Z.X. Mechanical alloying and electronic simulations of (MgH₂ + M) systems (M = Al, Ti, Fe, Ni, Cu and Nb) for hydrogen storage. *Int. J. Hydrog. Energy* **2004**, *29*, 73–80. [[CrossRef](#)]
28. Zaluski, L.; Zaluska, A.; Strrm-olsen, J.O.; Schulz, R. Catalytic effect of Pd on hydrogen absorption in mechanically alloyed Mg₂Ni, LaNi₅ and FeTi. *J. Alloys Compd.* **1995**, *217*, 295–300. [[CrossRef](#)]
29. Iturbe-garcía, J.L.; García-núñez, M.R.; López-muñoz, B.E. Synthesis of the Mg₂Ni Alloy Prepared by Mechanical Alloying Using a High Energy Ball Mill. *J. Mex. Chem. Soc.* **2010**, *54*, 46–50. [[CrossRef](#)]
30. Kumar, S.; Tiwari, G.P.; Krishnamurthy, N. High performance FeTi-3.1 mass% V alloy for on board hydrogen storage solution. *Energy* **2014**, *75*, 520–524. [[CrossRef](#)]
31. Andreasen, A. Hydrogenation properties of Mg–Al alloys. *Int. J. Hydrog. Energy* **2008**, *33*, 7489–7497. [[CrossRef](#)]
32. Gleiter, H. Nanostructured materials: Basic concepts and microstructure. *Acta Mater.* **2000**, *48*, 1–29. [[CrossRef](#)]
33. Friedrichs, O.; Kolodziejczyk, L.; Fernandez, A. Synthesis of nanocrystalline MgH₂ powder by gas-phase condensation and in situ hydridation: TEM, XPS and XRD study. *J. Alloys Compd.* **2007**, *435*, 721–724. [[CrossRef](#)]
34. Lopez-Suarez, A. Effect of absorption and desorption of hydrogen in Ti and Ti alloys. In *New Advances in Hydrogenation Processes: Fundamental and Applications*; Iran Polymer and Petrochemical Institute: Teheran, Iran, 2017. [[CrossRef](#)]
35. Parker, S.F.; Konrad, M.; Wieland, S.D. The effect of particle size, morphology and support commercial catalysts. *Chem. Sci.* **2019**, *10*, 480–489. [[CrossRef](#)] [[PubMed](#)]
36. Ismail, M.; Mustafa, N.S.; Yap, A.H. Catalytic effect of CeCl₃ on the hydrogen storage properties of MgH₂. *Mater. Chem. Phys.* **2016**, *170*, 77–82. [[CrossRef](#)]
37. Lototskyy, M.; Davids, M.W.; Pollet, B.G. Magnesium-based hydrogen storage nanomaterials prepared by high energy reactive ball milling in hydrogen at the presence of mixed titanium—iron oxide. *J. Alloys Compd.* **2015**, *645*, S454–S459. [[CrossRef](#)]

38. Bouaricha, S.; Dodelet, J.P.; Schulz, R. Hydriding behavior of Mg–Al and leached Mg–Al compounds prepared by high-energy ball-milling. *J. Alloys Compd.* **2000**, *297*, 282–293. [[CrossRef](#)]
39. Liang, G.; Huot, J.; Boily, S.; Van Neste, A.; Schulz, R. Hydrogen storage properties of the mechanically milled MgH₂–V nanocomposite. *J. Alloys Compd.* **1999**, *291*, 295–299. [[CrossRef](#)]
40. Huang, H.X.; Huang, K.L.; Liu, S.Q. Microstructures and electrochemical properties of Mg_{0.9}Ti_{0.1}Ni_{1-x}M_x (M = Co, Mn; x = 0, 0.1, 0.2) hydrogen storage alloys. *Powder Technol.* **2010**, *198*, 144–148. [[CrossRef](#)]
41. Vermeulen, P.; Niessen, R.A.H.; Notten, P.H.L. Hydrogen storage in metastable Mg_yTi_(1-y) thin films. *Electrochem. Commun.* **2006**, *8*, 27–32. [[CrossRef](#)]
42. Luo, W. (LiNH₂–MgH₂): A viable hydrogen storage system. *J. Alloys Compd.* **2004**, *381*, 284–287. [[CrossRef](#)]
43. Castro, F.J.; Fuster, V.; Urretavizcaya, G. Hydrogen sorption properties of a MgH₂–10wt. % graphite mixture. *J. Alloys Compd.* **2011**, *509*, S595–S598. [[CrossRef](#)]
44. Zhang, Y.; Zhang, W.; Qi, W.B.Y. A Comparison Study of Hydrogen Storage Thermodynamics and Kinetics of YMg₁₁Ni Alloy Prepared by Melt Spinning and Ball Milling. *Acta Metall. Sin.* **2017**, *30*, 1040–1048. [[CrossRef](#)]
45. Imamura, H.; Hashimoto, Y.; Sakata, Y. Preparation and Properties of Ball-Milled MgH₂/Al Nanocomposites for Hydrogen Storage. *Mater. Trans.* **2014**, *55*, 572–576. [[CrossRef](#)]
46. *CRYSTMET Database, version 5.0.0*; Toth Information Systems Inc.: Ottawa, ONT, Canada, 2013.
47. Lototsky, M.; Wafeeq, M.; Yartys, V.A. Nanostructured hydrogen storage materials prepared by high-energy reactive ball milling of magnesium and ferrovandium. *Int. J. Hydrog. Energy* **2019**, *44*, 6687–6701. [[CrossRef](#)]
48. Williams, M.; Lototsky, M.V.; Pollet, B.G. Hydrogen absorption study of high-energy reactive ball milled Mg composites with palladium additives. *J. Alloys Compd.* **2013**, *580*, s144–s148. [[CrossRef](#)]
49. Bhatnagar, A.; Pandey, S.K.; Srivastava, O.N. Catalytic effect of carbon nanostructures on the hydrogen storage properties of MgH₂–NaAlH₄ composite. *Int. J. Hydrog. Energy* **2014**, *39*, 14240–14246. [[CrossRef](#)]
50. Yahya, M.S.; Ismail, M. Catalytic effect of SrTiO₃ on the hydrogen storage behaviour of MgH₂. *J. Energy Chem.* **2019**, *28*, 46–53. [[CrossRef](#)]
51. Hanada, N.; Ichikawa, T.; Fujii, H. Remarkable improvement of hydrogen sorption kinetics in magnesium catalyzed with Nb₂O₅. *J. Alloys Compd.* **2006**, *420*, 46–49. [[CrossRef](#)]
52. Juahir, N.; Mustafa, N.S.; Sinin, A.M. Improved hydrogen storage properties of MgH₂ by addition of Co₂NiO nanoparticles. *RSC Adv.* **2015**, *5*, 60983–60989. [[CrossRef](#)]
53. Malka, I.E.; Pisarek, M.; Bystrzycki, J. A study of the ZrF₄, NbF₅, TaF₅, and TiCl₃ influences on the MgH₂ sorption properties. *Int. J. Hydrog. Energy* **2011**, *36*, 12909–12917. [[CrossRef](#)]
54. Wu, C.Z.; Wang, P.; Cheng, H.M. Hydrogen storage properties of MgH₂/SWNT composite prepared by ball milling. *J. Alloys Compd.* **2006**, *420*, 278–282. [[CrossRef](#)]
55. El-eskandarany, M.S.; Shaban, E.; Al-duweesh, A. Superior catalytic effect of nanocrystalline big-cube Zr₂Ni metastable phase for improving the hydrogen sorption / desorption kinetics and cyclability of MgH₂ powders. *Energy* **2015**, *91*, 274–282. [[CrossRef](#)]
56. Santos, S.F.; Ishikawa, T.T.; Huot, J. MgH₂ + FeNb nanocomposites for hydrogen storage. *Mater. Chem. Phys.* **2014**, *147*, 557–562. [[CrossRef](#)]
57. Liang, G.; Huot, J.; Boily, S.; Van Neste, A.; Schulz, R. Hydrogen storage in mechanically milled Mg–LaNi₅ and MgH₂–LaNi₅ composites. *J. Alloys Compd.* **2000**, *297*, 261–265. [[CrossRef](#)]
58. Chen, X.Q.; Podloucky, R.; Rogl, P. Computational and experimental study of phase stability, cohesive properties, magnetism and electronic structure of TiMn₂. *Acta Mater.* **2003**, *51*, 1239–1247. [[CrossRef](#)]
59. Erika, T.; Sebastian, C.; Fernando, Z. Temperature performance of AB₅ hydrogen storage alloy for Ni-MH batteries. *Int. J. Hydrog. Energy* **2016**, *41*, 19684–19690. [[CrossRef](#)]
60. Hayakawa, H.; Akiba, E.; Kohno, T. Crystal Structures of La–Mg–Ni_x (x = 3–4) System Hydrogen Storage Alloys. *Mater. Trans.* **2005**, *46*, 1393–1401. [[CrossRef](#)]
61. Boeije, M.F.J.; Delczeg-czirjak, E.K.; Brück, E. On the phase stability of CaCu₅-type compounds. *J. Alloys Compd.* **2017**, *722*, 549–554. [[CrossRef](#)]
62. Singh, A.; Singh, B.K.; Srivastava, O.N. Studies on improvement of hydrogen storage capacity of AB₅ type: MmNi_{4.6}Fe_{0.4} alloy. *Int. J. Hydrog. Energy* **2004**, *29*, 1151–1156.
63. Roberts, M.; Smith, R.I.; Hull, S. In situ investigation of commercial Ni(OH)₂ and LaNi₅-based electrodes by neutron powder diffraction. *J. Mater. Res.* **2015**, *30*, 407–416.
64. Cermak, J.; David, B. Catalytic effect of Ni, Mg₂Ni and Mg₂NiH₄ upon hydrogen desorption from MgH₂. *Int. J. Hydrog. Energy* **2011**, *6*, 3–9. [[CrossRef](#)]

65. Khajavi, S.; Rajabi, M.; Huot, J. Effect of cold rolling and ball milling on first hydrogenation of Ti_{0.5}Zr_{0.5}(Mn_{1-x}Fe_x)Cr₁, x = 0, 0.2, 0.4. *J. Alloys Compd.* **2019**, *775*, 912–920. [[CrossRef](#)]
66. Gkanas, E.I.; Khzouz, M.; Makridis, S.S. Synthesis and Hydrogen Sorption Characteristics of Mechanically Alloyed Mg(Ni_xMn_{1-x})₂ Intermetallics. *Mater. Sci.* **2017**, *12*, 257–268.
67. Srivastava, S.; Panwar, K. Effect of transition metals on ball-milled MmNi₅ hydrogen storage alloy. *Mater. Renew. Sustain. Energy* **2015**, *4*, 19. [[CrossRef](#)]
68. Broz, M.E.; Cook, R.F.; Whitney, D.L. Microhardness, toughness, and modulus of Mohs scale minerals. *Am. Mineral.* **2006**, *91*, 2006. [[CrossRef](#)]
69. Chen, Y.; Sequeira, C.A.C.; Song, X.; Neto, R.; Wang, Q. Polytypism of La–Ni phases in multicomponent AB₅ type hydride electrode alloys. *Int. J. Hydrog. Energy* **2002**, *27*, 63–68. [[CrossRef](#)]
70. Dobrovolsky, V.D. The correlation between ionicity of metal-hydrogen bonds in hydrides and their thermal firmness. In *Hydrogen Materials Science and Chemistry of Carbon Nanomaterials*; Springer: Dordrecht, The Netherlands, 2007; pp. 421–428.
71. Joseph, B.; Schiavo, B. Effects of ball-milling on the hydrogen sorption properties of LaNi₅. *J. Alloys Compd.* **2009**, *480*, 912–916. [[CrossRef](#)]
72. Kouloukakis, E.D.; Christodoulou, C.N.; Fruchart, D. High-Temperature Activated AB₂ Nanopowders for Metal Hydride Hydrogen Compression. *Int. J. Energy Res.* **2014**, *38*, 477–486. [[CrossRef](#)]
73. Ouyang, L.; Huang, J.; Zhu, M. Progress of hydrogen storage alloys for Ni-MH rechargeable power batteries in electric vehicles: A review. *Mater. Chem. Phys.* **2017**, *200*, 164–178. [[CrossRef](#)]
74. Stein, F.; Palm, M.; Sauthoff, G. Structure and stability of Laves phases. Part I. Critical assessment of factors controlling Laves phase stability. *Intermetallics* **2004**, *12*, 713–720. [[CrossRef](#)]
75. Hammerschmidt, T.; Ladines, A.N.; Drautz, R. Crystal-Structure Analysis with Moments of the Density-of-States: Application to Intermetallic Topologically Close-Packed Phases. *Crystals* **2016**, *6*, 18. [[CrossRef](#)]
76. Ioannidou, A.; Makridis, S.; Kikkinides, E.S. Structural and Hydrogenation Properties of Zr_{0.9}Ti_{0.1}Cr_{1.2-x}V_{0.8}Ni_x (x=0, 0.4) Compounds. *Mater. Sci. Forum.* **2010**, *636*, 26–31.
77. Liu, P.; Xie, X.; Liu, T. Hydrogen storage properties of (Ti_{0.85}Zr_{0.15})_{1.05}Mn_{1.2}Cr_{0.6}V_{0.1}M_{0.1} (M=Ni, Fe, Cu) alloys easily activated at room temperature. *Prog. Nat. Sci. Mater. Int.* **2017**, *27*, 652–657. [[CrossRef](#)]
78. Zhang, Y.; Xu, S.; Zhao, D. Hydrogen storage kinetics of nanocrystalline and amorphous Cu–Nd-added Mg₂Ni-type alloys. *Trans. Nonferrous Met. Soc. China* **2014**, *24*, 3524–3533. [[CrossRef](#)]
79. Liu, J.; Song, X.P.; Chen, G.L. Hydrogen storage performance of Mg-based composites prepared by spark plasma sintering. *J. Alloys Compd.* **2009**, *486*, 338–342. [[CrossRef](#)]
80. Becker, H. Processing of bulk Al7075 alloy by spark plasma sintering. *Mater. Sci. Eng.* **2017**, *179*, 2050.
81. Pei, P.; Song, X.; Liu, J.; Song, A.; Zhang, P.; Chen, G. Study on the hydrogen desorption mechanism of a Mg–V composite prepared by SPS. *Int. J. Hydrog. Energy* **2011**, *37*, 984–989. [[CrossRef](#)]
82. Huang, H.; Huang, K. Effect of Fluorination Treatment on Electrochemical Properties of M₁Ni_{3.5}Co_{0.6}Mn_{0.4}Al_{10.5} Hydrogen Storage Alloy. *J. Braz. Chem. Soc.* **2012**, *23*, 951–957.
83. Schwars, R.B.; Johnson, W.L. Formation of an amorphous alloy by solid-state reaction of the pure polycrystalline metals. *Phys. Rev. Lett.* **1983**, *51*, 415. [[CrossRef](#)]
84. Termsuksawad, P.; Niyomsoan, S.; Gavra, Z. Measurement of hydrogen in alloys by magnetic and electronic techniques. *J. Alloys Compd.* **2004**, *373*, 86–95. [[CrossRef](#)]
85. Zadorozhnyy, V.Y.; Milovzorov, G.S.; Kaloshkin, S.D. Preparation and hydrogen storage properties of nanocrystalline TiFe synthesized by mechanical alloying. *Prog. Nat. Sci. Mater. Int.* **2017**, *27*, 149–155. [[CrossRef](#)]
86. Møller, K.T.; Sheppard, D.; Ravnsbæk, D.B. Complex Metal Hydrides for Hydrogen, Thermal and Electrochemical Energy Storage. *Energies* **2017**, *10*, 1645. [[CrossRef](#)]
87. Song, X.; Zhang, P.; Chen, G. The role of spark plasma sintering on the improvement of hydrogen storage properties of Mg-based composites. *Int. J. Hydrog. Energy* **2010**, *35*, 8080–8087. [[CrossRef](#)]
88. Pei, P.; Song, X.P.; Chen, G.L. Improving hydrogen storage properties of Laves phase related BCC solid solution alloy by SPS preparation method. *Int. J. Hydrog. Energy* **2009**, *34*, 8597–8602. [[CrossRef](#)]
89. Lv, P.; Guzik, M.N.; Huot, J. Effect of ball milling and cryomilling on the microstructure and first hydrogenation properties of TiFe + 4 wt.% Zr alloy. *J. Mater. Res. Technol.* **2019**, *10*, 1016. [[CrossRef](#)]

90. Zhang, Q.A.; Zhang, L.X.; Wang, Q.Q. Crystallization behavior and hydrogen storage kinetics of amorphous $Mg_{11}Y_2Ni_2$ alloy. *J. Alloys Compd.* **2013**, *551*, 376–381. [[CrossRef](#)]
91. Zhang, D.Z.Y.; Li, B.; Ren, H.; Li, X.; Qi, T. Enhanced Hydrogen Storage Kinetics of Nanocrystalline and Amorphous Mg_2Ni -type Alloy by Melt Spinning. *Materials (Basel)* **2011**, *4*, 274–287. [[CrossRef](#)]
92. Wu, Y.; Lototsky, M.V.; Yartys, V.A. Microstructure and hydrogenation behavior of ball-milled and melt-spun $Mg-10Ni-2Mm$ alloys. *J. Alloys Compd.* **2008**, *466*, 176–181. [[CrossRef](#)]
93. Lass, E.A. Hydrogen storage measurements in novel Mg-based nanostructured alloys produced via rapid solidification and devitrification. *Int. J. Hydrog. Energy* **2011**, *36*, 10787–10796. [[CrossRef](#)]
94. Modibane, K.D.; Williams, M.; Lototsky, M. Poisoning-tolerant metal hydride materials and their application for hydrogen separation from CO_2/CO containing gas mixtures. *Int. J. Hydrog. Energy* **2013**, *38*, 9800–9810. [[CrossRef](#)]
95. Aguey-Zinsou, K.F.; Ares Fernandez, J.R.; Klassen, T. Effect of Nb_2O_5 on MgH_2 properties during mechanical milling. *Int. J. Hydrog. Energy* **2007**, *32*, 221–233.
96. Williams, M.; Nechaev, A.N.; Lototsky, M.V. Influence of aminosilane surface functionalization of rare earth hydride-forming alloys on palladium treatment by electroless deposition and hydrogen sorption kinetics of composite materials. *Mater. Chem. Phys.* **2009**, *115*, 136–141. [[CrossRef](#)]
97. Yeung, K.L.; Christiansen, S.C.; Varma, A. Palladium composite membranes by electroless plating technique Relationships between plating kinetics, film microstructure and membrane performance. *J. Memb. Sci.* **1999**, *159*, 107–122. [[CrossRef](#)]
98. Parambath, V.B.; Nagar, R.; Ramaprabhu, S. Effect of Nitrogen Doping on Hydrogen Storage Capacity of Palladium Decorated Graphene. *Langmuir* **2012**, *28*, 7826–7833. [[CrossRef](#)]
99. Charbonnier, M.; Romand, M.; Goepfert, Y. Palladium reduction: A key step for the electroless Ni metallization of insulating substrates by a tin-free process. *Thin Solid Film.* **2006**, *515*, 1623–1633. [[CrossRef](#)]
100. Shan, X.; Payer, J.H.; Jennings, W.D. Mechanism of increased performance and durability of Pd-treated metal hydriding alloys. *Int. J. Hydrog. Energy* **2009**, *34*, 363–369. [[CrossRef](#)]
101. Denys, R.V.; Lototsky, M.V.; Linkov, V.M.; Williams, M. Palladium mixed-metal surface-modified AB_5 -type intermetallics enhance hydrogen sorption kinetics. *S. Afr. J. Sci.* **2010**, *106*, 1–6.
102. Lototsky, M.V.; Williams, M.; Yartys, V.A. Surface-modified advanced hydrogen storage alloys for hydrogen separation and purification. *J. Alloys Compd.* **2011**, *509*, 555–561. [[CrossRef](#)]
103. Davids, W.; Lototsky, M.V.; Williams, M. Surface modification of TiFe hydrogen storage alloy by metal-organic chemical vapour deposition of palladium. *Int. J. Hydrog. Energy* **2011**, *36*, 9743–9750. [[CrossRef](#)]
104. Pasquini, L.; Callini, E.; Maurizio, C. Magnesium nanoparticles with transition metal decoration for hydrogen storage. *J. Nanoparticle Res.* **2011**, *13*, 5727–5737. [[CrossRef](#)]
105. Mark, I.; Doyle, L.; Benjamin, D. Hydrogen storage materials. *United States Pat.* **2000**, *6*, 165.
106. Modibane, K.D.; Lototsky, M.; Davids, M.W.; Williams, M.; Hato, M.J.; Molapo, K.M. Influence of co-milling with palladium black on hydrogen sorption performance and poisoning tolerance of surface modified AB_5 -type hydrogen storage alloy. *J. Alloys Compd.* **2018**, *750*, 523–529. [[CrossRef](#)]
107. Ceramics, M.; Skorokhod, V.V.; Klimenko, V.P. Reversible hydriding of $LaNi_{5-x}Al_x-Pd$ composite in the presence of carbon monoxide. *Powder Metall. Met. Ceram.* **2001**, *39*, 575–583.
108. Willey, D.B.; Pederzoli, D.; Harris, I.R. Low temperature hydrogenation properties of platinum group metal treated, nickel metal hydride electrode alloy. *J. Alloys Compd.* **2002**, *332*, 806–809. [[CrossRef](#)]

